Thermal Analysis of Cryoprotectants for Cryopreservation

A Thesis
SUBMITTED TO THE FACULTY OF
UNIVERSITY OF MINNESOTA
BY

Shaunak Shriharsh Phatak

IN PARTIAL FULFILLMENT OF THE REQUIREMENTS
FOR THE DEGREE OF
MASTER OF SCIENCE IN MECHANICAL ENGINEERING

Adviser: Dr. John. C. Bischof

February 2017

Acknowledgements

Firstly, I would like to express my sincere gratitude to my adviser, Dr. John Bischof. His guidance, patience and critical analysis helped in making this thesis a reality. I would also like to thank Harishankar Natesan for mentoring me through the course of this project. His advice and regular discussions helped in greatly improving this project. I am thankful to my research committee members, Dr. Cari Dutcher and Dr. Alena Talkachova for their valuable inputs and constructive questions about this work. I am thankful to Dr. Jeunghwan Choi and Dushyant Mehra for their advice regarding DSC experiments. I thank Dr. Navid Manuchehrabadi for his assistance in the thermal modeling part of this work. Also, I want to thank David Giles in the Chemical Engineering Department for his tutorial on DSC measurements. I also thank all my fellow lab mates Dr. Zhe Gao, Joel Scheumann, Kanav Khosla, Priyatanu Roy, Yiru Wang, Dr. Qi Shao, Li Zhan and Feng Liu for their help, teaching and critique of this work. Lastly, I thank my family for their patience and unconditional support. I also thank all the other people who I may have failed to mention at this time for their help and support during the course of this project. I am thankful for the funding provided for this work by the Center for Research in Education and Simulation Technologies at the University of Minnesota and the National Science Foundation (Award Number CBET 1236760).

Abstract

Cryopreservation by vitrification is a promising technique for preservation of biomaterials such as organs for long term storage. Crystallization while cooling and warming is an important hurdle for a successful cryopreservation. This problem can be addressed by the use of cryoprotectant solutions (CPAs) which help in inhibiting crystallization. The cooling and warming rates needed to prevent crystallization in these CPAs are called Critical Cooling Rate (CCR) and Critical Warming Rate (CWR) respectively. Thermal modeling is an important tool which can help to study this process and predict subsequent cooling and warming rates needed to avoid crystallization. Temperature dependent thermal properties such as thermal conductivity, specific heat capacity and density are needed in order to develop an accurate model. This work involved the measurement of specific heat capacity (C_p) of high concentration CPAs (> 6M) that are used to study vitrification. The thermal properties were then used in a numerical model to predict cooling and warming rates encountered in a cylindrical geometry of CPAs.

Chapter 1 provides a review of the thermal properties (thermal conductivity and specific heat capacity) of various biomaterials available in the literature in the sub-zero and supra-zero temperature ranges. Thermal properties of biomaterials are highly temperature dependent. In addition to dependence on temperature, these properties are affected by crystallization and vitrification at sub-zero temperatures (<0°C) and protein denaturation and water loss at supra-zero temperatures (>0°C). Finally, a modeling case study (Bischof and Han 2002) has been provided to highlight the significance of using temperature dependent thermal properties for accurately predicting thermal history.

Chapter 2 focusses on experimental measurements of specific heat capacity (c_p) of five high concentration CPAs (> 6M) — VS55 (with and without sucrose), DP6 (with and without sucrose) and M22. Further, the effect of cooling / warming rate (1, 5 and 10 °C/min) on crystallization and vitrification has been studied. It was observed that the addition of 0.6 M sucrose to two CPAs viz., VS55 and DP6 suppressed their crystallization for all the three cooling and warming rates.

Chapter 3 involves thermal modeling of cooling and warming in a COMSOL Multiphysics package. Thermal properties from Chapters 1 & 2 were used in order to predict the cooling and warming rates for three conditions, viz. convective cooling, convective warming and nano warming. These simulations were carried out in a cylindrical geometry for an increasing size, i.e. the radius of the cylinder. The objective was to find the size limit beyond which cooling and warming rates would not exceed the CCR and CWR respectively.

Table of Contents

Acknowledgements i
Abstract ii
Table of Contents iii
List of Tables v
List of Figures vi
Appendix List of Tables vii
Appendix List of Figures viii
Chapter 1: Thermal Properties of Porcine and Human Biological Systems 1
1.1 Introduction 1
1.2 Thermal Properties 3
1.2.1 Thermal Conductivity Measurement 4
1.2.2 Specific Heat Capacity Measurement 5
1.3 Factors that Affect Thermal Property values 7
1.3.1 High Temperature Effects (37 °C – 100 °C): Protein Phase Change and Water Loss 8
1.3.2 Low temperature effects (37 °C – -196 °C): Water Phase change and Cryoprotectant Effects 9
1.4 Modeling Case Study 12
1.5 Conclusion 16
Chapter 2: DSC Measurements of Cryoprotectants (CPAs) 17
2.1 Introduction 17
2.2 Materials and Methods 20
2.2.1 CPA Solutions 20
2.2.2 Differential Scanning Calorimetry (DSC) 21
2.3 Results and Discussion 25
2.4 Conclusion 33
Chapter 3: Thermal Modeling of Cryoprotectants (CPAs) to study Vitrification 34
3.1 Introduction 34
3.2 Methods 35
3.3 Results and Discussion 38
3.4 Conclusion 43
Appendix 44
Appendix A 50
Appendix B 58
B.1 DSC Protocol for Maximal Crystallization Measurements 58

B.2 DSC c_p Datasets of CPAs not shown in Chapter 2. 60
Appendix C 63
C.1 Convective Cooling Results for VS55 and DP6 with 0.6 M Sucrose 63
C.2 Convective Warming Results for VS55 and DP6 with 0.6 M Sucrose. 64
C.3 Nano-Warming Results for VS55 and DP6 with 0.6 M Sucrose using msIONP 64
C.4 Nano-Warming Results for all CPAs using EMG308 Nano-particles. 65

List of Tables

Table 1. Overview of Common Bioheat transfer Applications 3
Table 2. Overview of ‘k’ measurement techniques 6
Table 3. Current Availability of Data for CPAs 20
Table 4. Thermal parameters of CPAs 26
Table 5. Crystallization Summary of CPAs 32
Table 6. Geometry Dimensions and Target Biomaterials for the Model 34
Table 7. SAR and Heat Generation Values 37
Table 8. Centre Cooling Rates for Convective Cooling 38
Table 9. Centre Warming Rates for Convective Warming 39
Table 10. Centre Warming Rates for Nano-Warming with msIONP 41

List of Figures

Figure 1. Schematic of most thermal conductivity measurement techniques. 4
Figure 2. Thermal Conductivity Datasets in the Suprazero Range 7
Figure 3. Thermal Conductivity Datasets in the sub-zero and cryogenic range 8
Figure 4. Specific Heat Capacity for biomaterials without cryoprotectants 9
Figure 5. Thermal Conductivity Datasets for porcine liver with and without cryoprotectants 10
Figure 6. Specific Heat Capacity for porcine liver with and without cryoprotectants 11
Figure 7. Thermal Conductivity Datasets for cryoprotectants 12
Figure 8. Thermal Properties of Water used for Modeling Case Study. 13
Figure 9. Geometry in Cylindrical Co-ordinates 14
Figure 10. Numerical Simulation for Cryopreservation 14
Figure 11. Numerical Simulation for Cryosurgery 15
Figure 12. Phase Diagram of Glycerol in Water 18
Figure 13. Specific Heat Capacity (c_p) for varying concentrations of glycerol 19
Figure 14. Schematic of a Heat Flux type DSC 21
Figure 15. Slope differences between literature and experimental Cp of Water 22
Figure 16. Thermogram for maximal crystallization 23
Figure 17. Thermogram for minimal crystallization 24
Figure 18. Thermogram for intermediate crystallization 25
Figure 19. Specific Heat Capacity (c_p) of VS55 for maximal and minimal crystallization 26
Figure 20. Calculation of c_p in the Melting Region 27
Figure 21. Thermogram for M22 28
Figure 22. Specific Heat Capacity (c_p) of M22 29
Figure 23. Thermogram for VS55 + 0.6 M Sucrose 30
Figure 24. Specific Heat Capacity (c_p) of VS55 and VS55 + 0.6 M Sucrose 31
Figure 25. Problem Geometry and Boundary Conditions 35
Figure 26. Nano-Warming Coil (15 kW) 36
Figure 27. Effect of ‘h’ on cooling rates in VS55 for convective cooling 39
Figure 28. Effect of thermal properties on cooling rates during convective warming 40
Figure 29. Convective Warming Vs Nano-Warming at a Time of 20 sec 40
Figure 30. Effect of power input on warming rates for nanowarming in VS55 41
Figure 31. Effect of power input on warming rates for nanowarming in DP6 42

Appendix List of Tables

Appendix Table 1. Organization of thermal property datasets 50
Appendix Table 2. Thermal Properties of Porcine Systems at sub-zero temperatures I 51
Appendix Table 3. Thermal Properties of Porcine Systems at sub-zero temperatures II 52
Appendix Table 4. Thermal Properties of Porcine Systems at supra-zero temperatures 53
Appendix Table 5. Thermal Properties of Human Systems at supra-zero temperatures I 54
Appendix Table 6. Thermal Properties of Human Systems at supra-zero temperatures II 55
Appendix Table 7. Thermal Properties of Cryoprotectants 56
Appendix Table 8. Thermal Properties of Porcine Liver treated with cryoprotectants 57
Appendix Table 9. Centre Cooling Rates for Convective Cooling 63
Appendix Table 10. Centre Cooling Rates for Convective Warming 64
Appendix Table 11. Centre Warming Rates for Nano – Warming with msIONP 64
Appendix Table 12. Centre Warming Rates for Nano – Warming with EMG308 65

Appendix List of Figures

Appendix Figure 1. Thermogram for maximal crystallization 58
Appendix Figure 2. Specific Heat Capacity (c_p) of DP6 for maximal and minimal crystallization 60
Appendix Figure 3. Specific Heat Capacity (c_p) of DP6 and DP6 + 0.6 M Sucrose 61
Appendix Figure 4. Specific Heat Capacity (c_p) for maximal crystallization measurements 62
Appendix Figure 5. Specific Heat Capacity (c_p) for minimal crystallization measurements 63

Chapter 1: Thermal Properties of Porcine and Human Biological Systems[1]

1.1 Introduction

Bioheat transfer, a key component in the field of thermal medicine, has traditionally been important to understand for the purpose of two main areas: thermal therapies and bio- or cryopreservation. Thermal therapy is the application of hot or cold temperatures to destroy undesirable tissues, such as tumors within the body (Sapareto and Dewey 1984; Chu and Dupuy 2014). Cryopreservation is the preservation of biomaterials for a number of applications, such as organ transplantation, in vitro fertilization, and food preservation, through cooling systems to very low temperatures (<-80°C) to arrest biological activity (Karlsson and Toner 1996). Cryopreservation can be achieved by slow freezing where addition of cryoprotectants such as glycerol and Dimethyl sulfoxide (DMSO) avoids intracellular ice formation or by fast cooling techniques that result in vitrification or glass formation due to the presence of cryoprotectants. Successful organ banking through cryopreservation would increase the number of possible transplantations; currently 1 in 5 patients die due to lack of an availability of viable organs (OPTN). More information regarding these applications can be found in the references provided in Table 1. More recently, interest in the thermal properties of human tissues has increased for the purpose of the development of predictive models for training and assessment of skills related to thermally related interventions and conditions.

For all applications of bioheat transfer, the temperature excursions of the biomaterials can be correlated to the injury that may occur in the system (He and Bischof 2003). Thus, thermal modeling is necessary to predict the thermal history and hence the injury, since it may not be always possible to measure temperature experimentally. Hence, analytical or numerical models become valuable in order to study the process. In cryopreservation, knowledge about thermal history and cooling rates will help in understanding the phases through which a particular system passes, i.e. liquid, crystal and glassy/vitreous states. The cooling and heating rates encountered in these systems can help define whether a system will pass through these various phases. Temperature gradients experienced due to fast cooling required for vitrification also affect stress development

[1] **This Chapter has been submitted for publication in the Handbook of Thermal Science and Engineering by Springer. It has been reproduced here with minor formatting changes.**

in the sample and can cause cracking. For more information on these topics, please see (Fahy et al. 1984; Rabin et al. 1998; Choi and Bischof 2010). In the case of cryosurgery, thermal history again would be an indicator of destruction of the tissue or tumor in the biological system. Mechanisms believed to cause damage include direct cell injury, vascular injury and immunological injury. These injuries depend upon the cooling and thawing rates, the minimum end temperatures and the hold times at these temperatures. As an example, tumor destruction is associated with a minimum lethal temperature. A heat transfer model can help understand these temperature distributions and cooling and heating rates, so as to correlate with actual experimental results (Rabin and Shitzer 1998; Etheridge et al. 2013). The interested reader is directed to (Rubinsky 2000; Hoffmann and Bischof 2002; Baust and Gage 2005; Sabel 2009) for more details regarding the injury mechanisms associated with cryosurgery. During thermal therapy, heating results in water loss and protein denaturation (Choi et al. 2013). These events lead to reduction in the thermal conductivity and specific heat capacity of the system of interest. Thus, temperature dependent thermal properties are needed when used in a model, as these directly will affect the thermal histories. For more information regarding the effects of higher temperatures on thermal properties, please refer to (Choi et al. 2013; Rossmann and Haemmerich 2014).

Heat transfer in biological systems is a complex process influenced by a variety of mechanisms: for example, conduction within tissues; convection as well as perfusion due to blood circulation; metabolic heat generation; heat exchange between different blood vessels and also thermoregulation effects including shivering; and vasodilation. An example is the classic Pennes Bioheat Equation (Pennes 1948):

$$\rho c_p \frac{\partial T}{\partial t} = \frac{\partial}{\partial x}\left(k \frac{\partial T}{\partial x}\right) + \dot{q}_m + \dot{q}_p$$

Where $\rho, c_p, T, k \; and \; \dot{q}_m$ are the tissue density, specific heat capacity, temperature, thermal conductivity and metabolic heat generation per unit volume. Energy exchange between blood and tissue is denoted by the perfusion term $\dot{q}_p$ given as follows-

$$\dot{q}_p = \omega \rho_b c_{pb} (T_a - T)$$

Where $\rho_b \; and \; c_{pb}$ are blood density and specific heat capacity respectively, ω is the perfusion rate and T_a is the arterial blood temperature. As seen in the Pennes equation, the tissue thermal properties (i.e. density, specific heat capacity and thermal conductivity) need to be determined in order to obtain the thermal history of the system for the above mentioned applications.

In addition to Pennes equation, many other models have been formulated to study these processes. In order to formulate these heat transfer models, readers may refer to (Charny 1992; Diller 1992; Arkin et al. 1994; Baish 2000).

Table 1. Overview of Common Bioheat transfer Applications

	Application	Temperature	Definition	Rep. ref.*
Biopreservation	Vitrification	<-140 °C	Preservation by attaining a glassy state	(Fahy et al. 1984; Song et al. 2000)
	Freezing	<-20 °C	Preservation by freezing in presence of cryoprotectants	(Mazur 1984; Karlsson and Toner 1996)
	Lyophilization/ Freeze Drying	<-20 °C	Preservation by drying after freezing	(Crowe et al. 1992; Carpenter et al. 1997)
	Hypothermic preservation	0 to 37 °C	Preservation at temperatures between 0 ^{0}C and 37 ^{0}C	(Belzer and Southard 1988; Steponkus 1996)
Biodestruction	Cryotherapy/ Cryoablation	<-20 °C	Destruction of tissue by freezing	(Gage and Baust 1998; Hoffmann and Bischof 2002)
	Mild hyperthermia	37 to 45 °C	As an adjuvant to sensitize tumors to radiation and chemotherapy	(Sapareto and Dewey 1984)
	Thermal ablation	>50 °C	Destruction of tissue by heating	(O'Neal et al. 2004)

*Representative reference. Table 1 has been reproduced from (Natesan and Bischof 2016) and permission has been requested.

1.2 Thermal Properties

Thermal properties focused in this chapter include thermal conductivity and specific heat capacity. Following are brief discussions on their measurement techniques-

1.2.1 Thermal Conductivity Measurement

Thermal conductivity (k, W/m-K) is a material property, a measurement of its ability to conduct heat. It is influenced by composition (i.e. water, lipid, proteins, and added cryoprotectants), phase (i.e. liquid, crystalline and amorphous phases), and temperature. Some methods used to measure thermal conductivity of biomaterials have been given in Table 2. These measurements use either

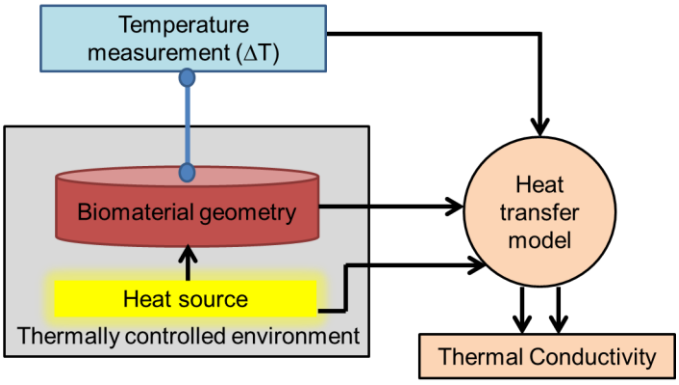

Figure 1. Schematic of most thermal conductivity measurement techniques. Figure 1 has been reproduced from (Natesan et al. 2016a) and permission has been requested.

a known heat flux or a known temperature gradient as depicted in the Figure 1. Thermal conductivity measurement techniques can be divided into two types: steady state and transient methods. In the case of steady state methods, information about heat flux and temperature response from the sample is used in a heat transfer model in order to calculate thermal conductivity. Some drawbacks of these methods include long times (~ several hours depending on sample size) are needed to reach steady state and a proper "guarding" is needed to prevent heat losses, thus leading to a need for a 1-D heat transfer model. Another problem with these methods is that of contact resistance between the sample and energy source.

As compared to steady state techniques, transient methods can be performed quickly (< 1 minute). For these methods, a cylindrical or spherical probe can be inserted into the sample to supply heat as well as measure temperature simultaneously. Although faster than steady state methods, these techniques also suffer from the problem of contact resistance between the sample and probe. The heat flow thus needs to penetrate deeper into the sample leading to negligible contact resistance at long time scales of heating. This necessitates a size requirement of >10 mm thus restricting these techniques for use in thick samples. Also being invasive, they may cause tissue damage.

Lastly, a recent method used for thermal conductivity is the 3ω method which belongs to a third category called as a "quasi-steady" technique. In this case a thin gold heater line is micro-fabricated on to a glass substrate. The measurement times for this method are in the range of tens of minutes

and can handle sample sizes in the range 0.1 mm to 2 mm. These methods have been reviewed previously in the following references: (Diller et al. 2000; Choi and Bischof 2010; Natesan et al. 2016a)

1.2.2 Specific Heat Capacity Measurement

Specific heat capacity (c_p, J/g-°C) is a material property that denotes the amount of heat that should be transferred to a material to raise its temperature by unit temperature (eg. degree Celsius). In the case of biomaterials, it is important to measure their Cp as a function of temperature. For example, in a wide temperature range (say -150 °C to 20 °C), cryoprotectants pass through different states, such as liquid, ice and vitrified (amorphous), with each of these phases having a different c_p, thus necessitating temperature dependent properties. The most common technique used to measure c_p is differential scanning calorimetry (DSC). DSC is capable of measuring c_p as well as latent heat of relatively small sample sizes (~3-100 mg) over a wide temperature range of -180°C to 750°C(Natesan and Bischof 2016). The technique measures the difference in the heat flow rate to the sample and reference pans while maintaining the same temperature program (Höhne et al. 1996).The reference sample has known thermal properties. This difference in heat flow can then be plotted as function of temperature or time. Using this measured differential heat flow($\emptyset_{sample}$) , the c_p can then be calculated as follows-

$$c_p = \frac{1}{m}\frac{d\emptyset_{sample}}{dt}.\frac{dt}{dT}$$

In terms of the heating technique used, there are two types of conventional DSC viz. standard DSC with linear heating and modulated DSC (M-DSC) with modulated heating. In the case of standard DSC, the sample and reference are heated through a linear temperature program. There are two types of standard DSC viz. the heat flux (HF) DSC and the power compensated (PC) DSC. The HF DSC consists of a single furnace area in which the sample and reference pans are loaded and temperatures measured with thermocouples. The temperature difference between the sample and reference pans is then used to calculate the differential heat flow. For a PC DSC, there are two separate furnaces wherein the sample and reference pans are loaded separately. The principle of this DSC, as well as its differentiator from the HF DSC, is that the temperature difference between sample and reference pans is kept zero by increasing or decreasing the heat flow to the sample in the event of a transition (e.g. phase change from water to ice) in the sample. For reliable measurements, it is necessary to calibrate the DSC, which usually consists of three steps: baseline calibration (accounts for instrument discrepancies); temperature calibration

(considers differences between measured and actual values of transition temperatures); and heat flow calibration (calculates a factor to correct differences between measured and actual heat flow rates). In the case of M-DSC, two simultaneous heating rates are used, i.e. a sinusoidal heating

Table 2. Overview of 'k' measurement techniques

Technique	Heat Source	Temperature Measuremen	Heat Transfer Model	Directionality	Reference
Guarded Hot Plate Method	Thermal	Thermocouple	Steady state 1-D Longitudina	Cross-plane	(Hill et al. 1967; Poppendiek et al. 1967)
Thermal Comparator	Thermal	Probe (Effective TC)	Transient 1-D Cylindrical	Not sensitive	(Vendrik and Vos 1957; Morley 1966; Vachon et al.
Radial Heat Flow Method	Thermal	Thermocouple (TC)	Steady state 1-D Cylindrical	In-plane	(Glassbrenner and Slack 1964)
Heated Thermocouple Method	Electrical	Thermocouple (TC)	Transient 1-D Spherical	Not sensitive	(Grayson 1952)
Transient Hot Wire Method	Electrical	Thermocouple (TC)	Transient 1-D Cylindrical	Not sensitive	(Bhattacharya and Mahajan 2003; Ehrlich et al. 2015)
Chato's Probe	Electrical	Thermocouple (TC)	Transient 1-D Spherical	Not sensitive	(Chato 1968; Balasubramaniam and Bowman 1977)
Pulse Decay	Electrical (Single Pulse)	Thermocouple (TC)	Transient 1-D Spherical	Not sensitive	(Chen et al. 1981; Valvano et al. 1985; Patel et al. 1987)
3ω	Electrical	3rd Harmonic Voltage Response	Quasisteady 1-D Cylindrical	Radial (bulk samples); cross-plane (thin	(Cahill and Pohl 1987; Lubner et al. 2015)

Table 2 has been reproduced from (Natesan et al. 2016a) and permission has been requested.

rate along with a linear heating rate. This DSC is capable of simultaneously measuring both the c_p of the sample as well as kinetic processes such as phase change (Reading et al. 1993; Marcus and Reading 1994; Reading et al. 1994; Natesan and Bischof 2016). The linear rate provides information similar to the standard DSC whereas the sinusoidal rate is useful for measuring the c_p

of the sample. The limitation of conventional DSC is the comparatively low scanning rates (<750°C/min) associated with it. For example, while studying vitrification (glass formation) of dilute cryoprotectants, a very high cooling rate is needed to vitrify the system without causing crystallization, and this cannot be attained in a conventional DSC. This limitation can be addressed by the development of nanocalorimetry (Yi et al. 2014) on a silicon-based membrane that can work with a very small sample weight (~ 10 ng), which leads to the possibility of very high heating or cooling rates (~10^7 °C/min).

1.3 Factors that Affect Thermal Property values

The focus of this chapter is on organizing literature data for thermal conductivity and specific heat capacity of human and porcine systems in the cryogenic, subzero and suprazero temperature ranges. All the data provided here has resulted from actual measurements presented in primary research

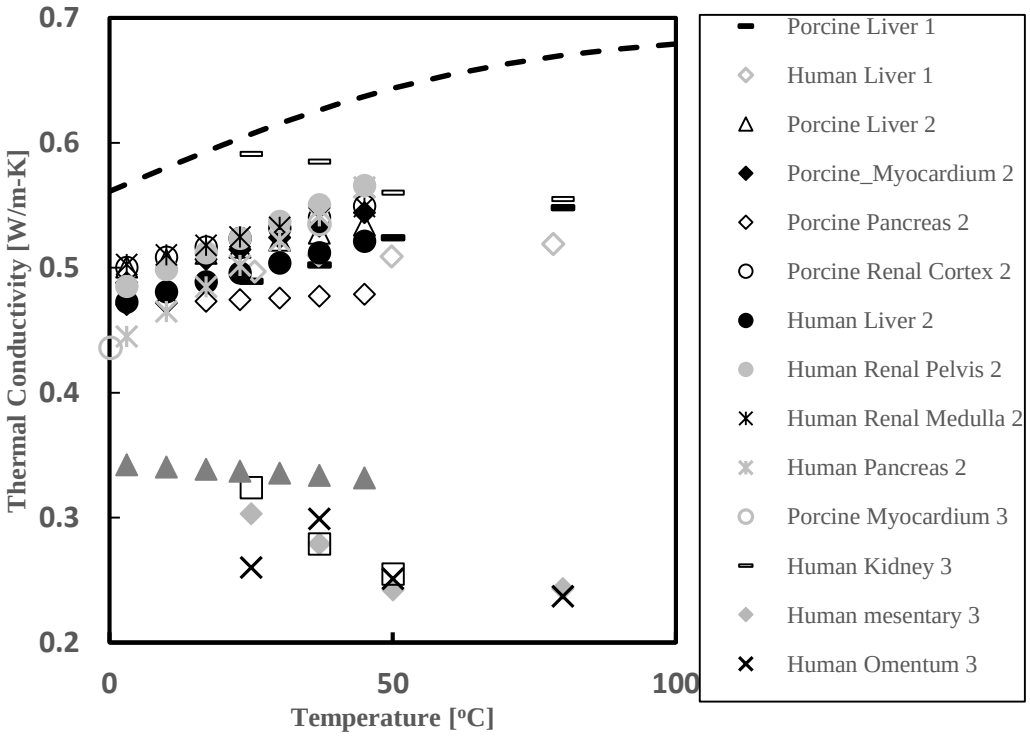

Figure 2. Thermal Conductivity Datasets in the Suprazero Range
where '1' refers to (Choi et al. 2013)**,** '2' refers to (Valvano et al. 1985) and '3' refers to Choi et al., unpublished listed in Appendix Tables 4, 5 and 6

papers. Apart from primary papers, there are some databases available such as the one by IT'IS Foundation associated with ETH Zurich (Hasgall et al. 2015) . In addition there are reviews on this topic such as (Bowman et al. 1975; Diller et al. 2000; Duck 2013). Blood perfusion results have not been taken into account in the data presented in this chapter. The interested reader may refer to

(Valvano 1995; Yuan et al. 1998; Diller et al. 2000; Liu et al. 2000; Bhattacharya and Mahajan 2003) for details regarding perfusion associated measurements.

Some factors that influence the thermal properties of biomaterials are discussed below-

1.3.1 High Temperature Effects (37 °C – 100 °C): Protein Phase Change and Water Loss

In the case of high temperatures, as seen in Figure 2, the values of thermal properties generally rise from 0 °C up to roughly 45 °C where protein denaturation and water loss can play a role. After 45 °C there is much less data, although it would appear that water loss plays a more prominent role as compared to protein denaturation resulting in lower values of 'k' and 'c_p'. This drop in thermal conductivity can be seen in Figure 2 above for human kidney, mesentery, omentum and gerota's fascia. The lower 'k' values for mesentery, gerota's fascia, omentum are due to a higher fat content in these systems. Similarly, human fat of spleen also exhibits lower 'k'

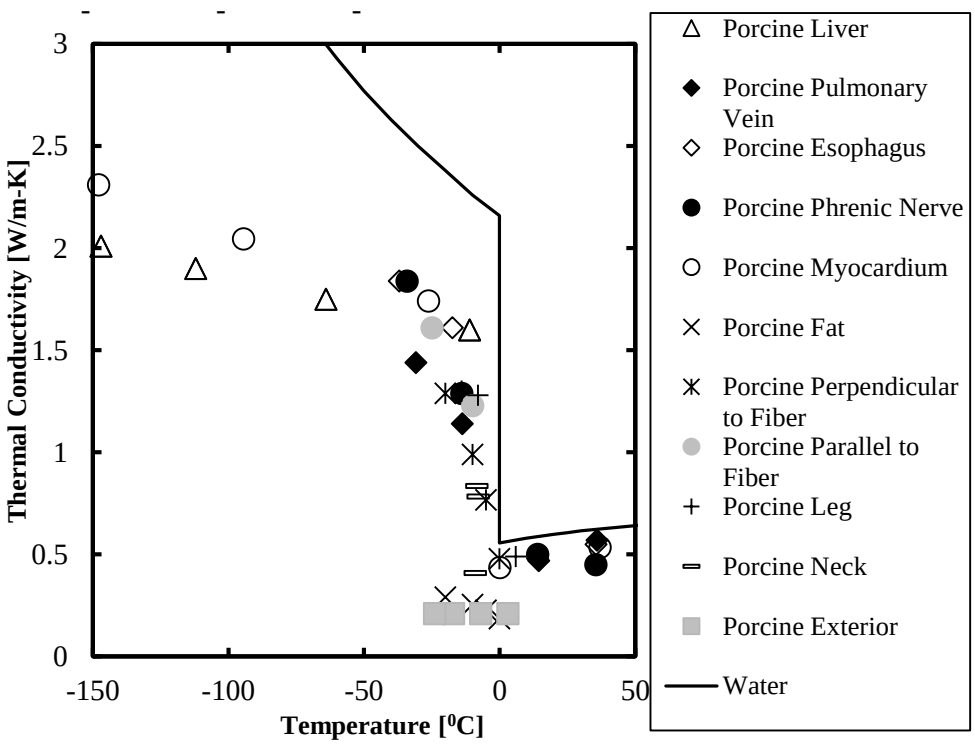

Figure 3. Thermal Conductivity Datasets in the sub-zero and cryogenic range
(datasets have been listed in Appendix Tables. 2 and 3)

values due to the presence of fat in the system. Protein denaturation occurs as a heat absorption event over a finite temperature range. The interested reader may refer to (Bhattacharya and

Mahajan 2003; Guntur et al. 2013; Choi et al. 2013) for more details regarding these high temperature effects.

1.3.2 Low temperature effects (37 °C – -196 °C): Water Phase change and Cryoprotectant Effects

Thermal properties of biomaterials at low temperatures are affected by two factors: phase change (water to ice) and the presence of cryoprotectants. Freezing or crystallization of water to ice results in an increase in thermal conductivity values at subzero temperatures as ice has a higher thermal conductivity compared to water. This general trend of increasing values of thermal conductivity can be observed in Figure 3 above for various biomaterials. In contrast, specific heat

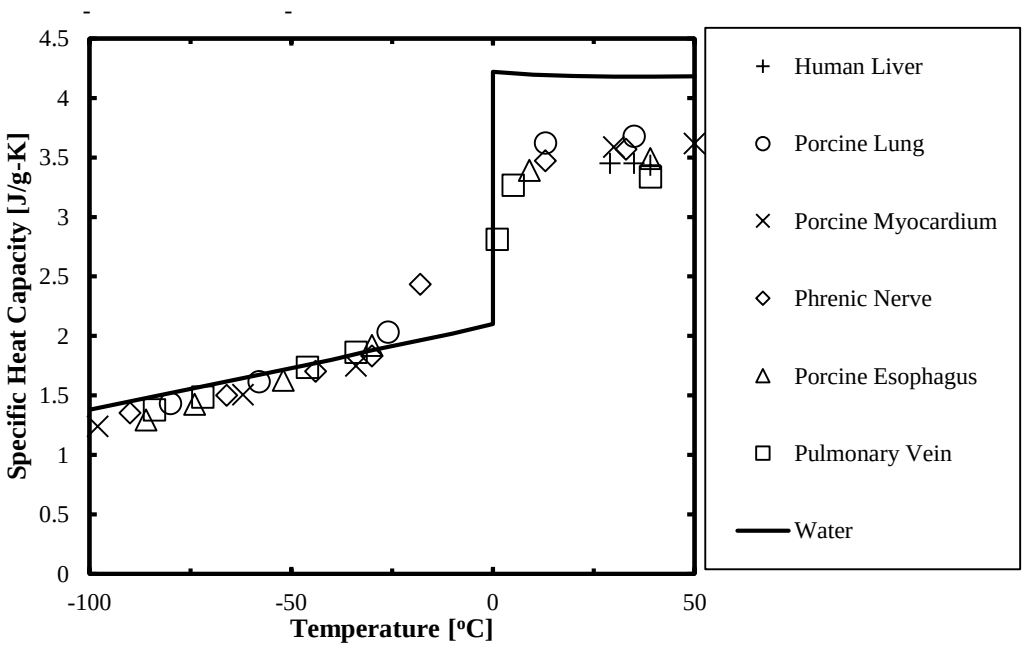

Figure 4. Specific Heat Capacity for biomaterials without cryoprotectants
(datasets have been listed in Appendix Tables. 2, 3 and 4).

capacity values show lower values at subzero temperatures as ice has a lower specific heat capacity when compared to water. This general trend of decreasing values of specific heat capacity for various biomaterials can be observed in Figure 4 below. The values of both thermal conductivity and specific heat capacity of most biomaterials are lower than those of water. The amount by which these values differ with respect to water depends upon the water content in these systems.

In addition to freezing effects, thermal properties of biomaterials are also affected by the presence of cryoprotectants. At lower temperatures (< -100°C), the systems experience glass transition, i.e. formation of a glassy or vitreous state due to cryoprotectants. Both thermal conductivity and specific heat capacity values are lowered due to this glass formation in the system. As seen in Figure 5 below, thermal conductivity values for porcine liver treated with various concentrations

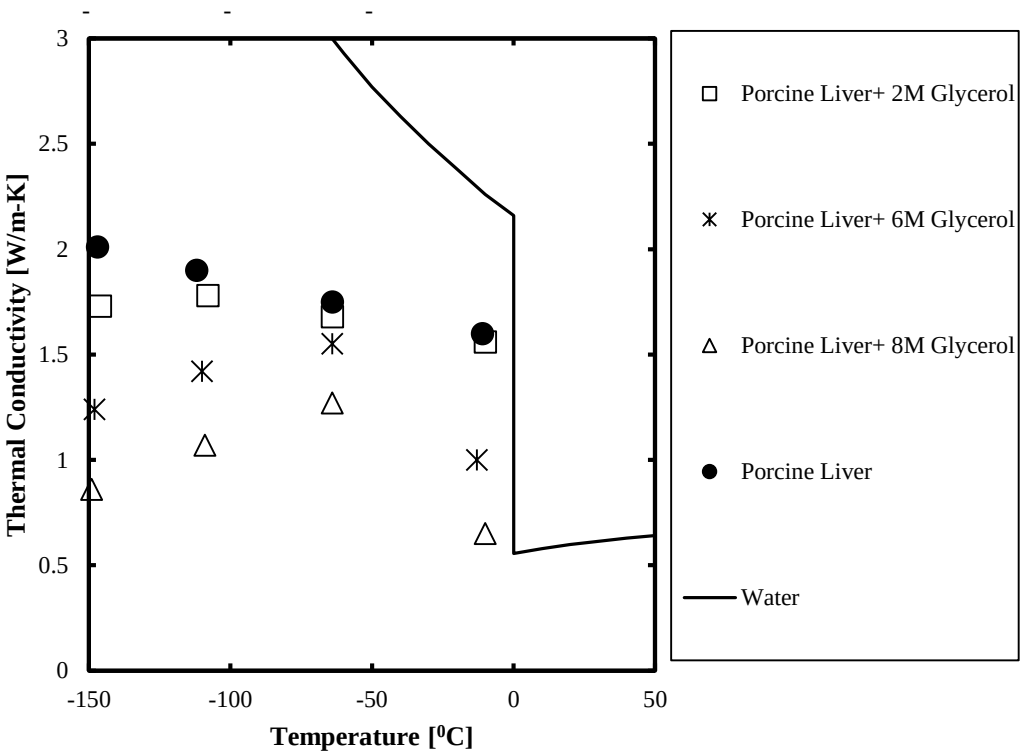

Figure 5. Thermal Conductivity Datasets for porcine liver with and without cryoprotectants
(datasets have been listed in Appendix Tables 3 and 8). Figure 5 has been reproduced from (Choi and Bischof 2008a) and permission has been requested.

of glycerol are lower as compared to porcine liver without any glycerol and continue to drop with higher concentrations of glycerol. The freezing or crystallization effects which tend to increase thermal conductivity are suppressed at lower temperatures in the presence of cryoprotectants which results in these lower thermal conductivity values.

In the case of specific heat capacity, as mentioned above, the values drop in the presence of cryoprotectants (-150°C to -100°C) due to the formation of the glassy or vitreous phase. Further, glass transition effects can be seen as a slight jump in the specific heat capacity values around -100°C in Figure 6 above. This jump results from the conversion of the glassy phase to a liquid phase. Beyond glass transition, the rise in values at higher temperatures is initially due to

conversion of the glassy phase to a liquid phase as mentioned above and later due to melting of the ice present in the system to water knowing that the specific heat capacity of water is greater than ice as well as the glassy phase.

Figure 7 below consists of thermal conductivity datasets for a number of cryoprotectants that can be useful when performing heat transfer simulations for cryopreservation.

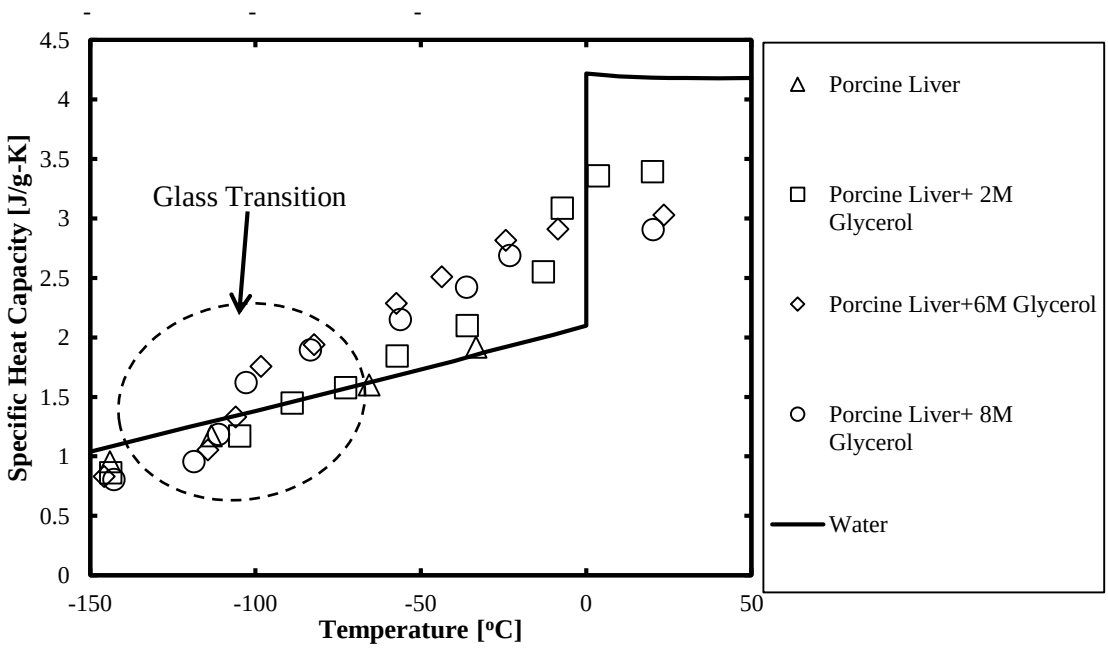

Figure 6. Specific Heat Capacity for porcine liver with and without cryoprotectants (datasets have been listed in Appendix Tables. 3 and 8). Figure 6 has been reproduced from (Choi and Bischof 2008a) and permission has been requested.

In addition, data has also been provided for Ultra Sound Gel (US Gel) which can be used as tissue phantom in the absence of property data for the required biomaterial. The general trends seen in Figure 7 are same as those observed in the case of porcine liver treated with glycerol in Figure 5. The thermal conductivity values increase at lower temperatures due to ice formation whereas the presence of the glassy phase due to cryoprotectants at temperatures < -100°C results in lower or constant thermal conductivity values. Also, as the concentration of cryoprotectants increases, the thermal conductivity values are lowered as the ice formation is suppressed by the glassy phase. These trends can be seen in Figure 7 for DMSO and glycerol. The interested reader is directed to (Zhang et al. 2002; Choi and Bischof 2008a; Ehrlich et al. 2016) for more discussion regarding low temperature and cryoprotectants related 'k' and 'c_p' measurements.

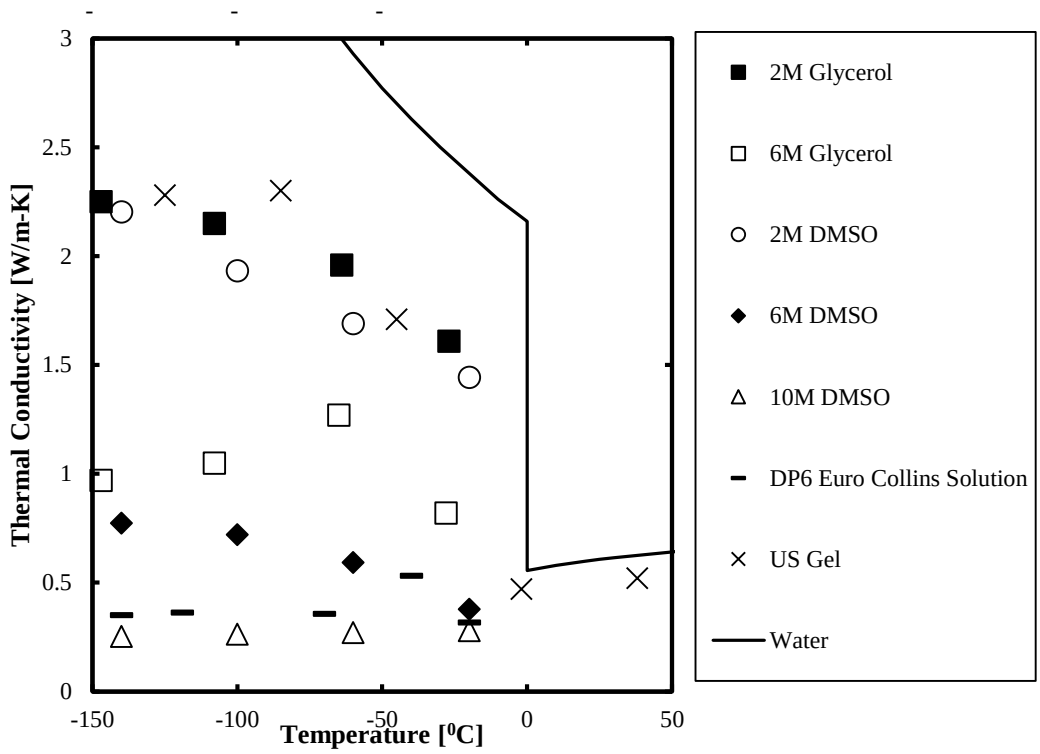

Figure 7. Thermal Conductivity Datasets for cryoprotectants
(datasets have been listed in Appendix Table. 7)

1.4 Modeling Case Study

This section provides an example from (Bischof and Han 2002) showing the importance of temperature dependent properties for numerical predictions of heat transfer applied for cryopreservation and cryosurgery. A numerical technique known as the Enthalpy method has been used to solve the heat transfer with phase change problem for cryopreservation and cryosurgery. The governing equation for this method (Ozisik 1994) is given as follows:

$$\rho \frac{\partial H(T)}{\partial t} = \nabla \cdot (k \nabla T) + g(T)$$

Where $\rho, H, T, t, k \; and \; g(T)$ are density, enthalpy, temperature, time, thermal conductivity and heat generation per unit volume.

The above equation is a modified version of the transient heat equation where enthalpy and temperature are dependent variables. In other techniques used for solving phase change, such as source tracking method, two equations are needed to solve for the frozen and unfrozen region. In addition, an energy balance equation is included to track the interface between these two regions. The advantage of the enthalpy method over such methods is that a single equation in terms of

enthalpy is used to solve for both regions and thus no tracking equation is needed. In the case of pure materials like water, phase change happens at a single temperature whereas for biomaterials, phase change occurs over a temperature range called a mushy zone. The enthalpy method can be used to solve for both these materials.

For information regarding this method and its applicability to cryosurgery and cryopreservation, readers may refer to (Zhang et al. 2005; Choi and Bischof 2010; Etheridge et al. 2013)

Constant as well as temperature dependent thermal properties of water have been used in these analyses.

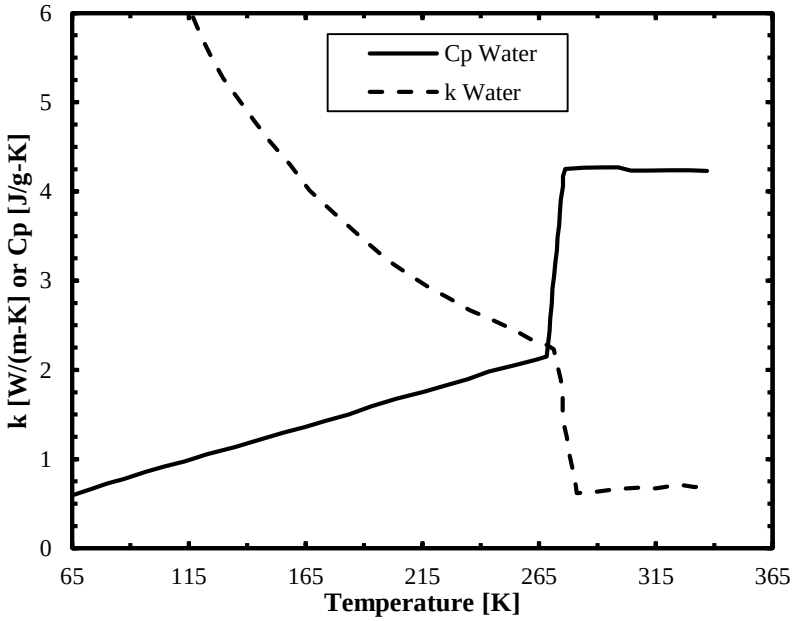

Figure 8. Thermal Properties of Water used for Modeling Case Study.
Figure 8 has been reproduced from (Bischof and Han 2002) and permission has been requested.

The thermal properties of water used in this analysis are provided in Figure 8 (Bald and Fraser 1982). As shown in Figure 9 below, an important distinction between cryopreservation and cryosurgery is that they have opposite boundary conditions, i.e. cryopreservation involves cooling from outside to the center of the system where a symmetric boundary condition can be applied; whereas cryosurgery involves freezing from the center with a probe to the surface where a temperature boundary condition (human body temperature) is applied.

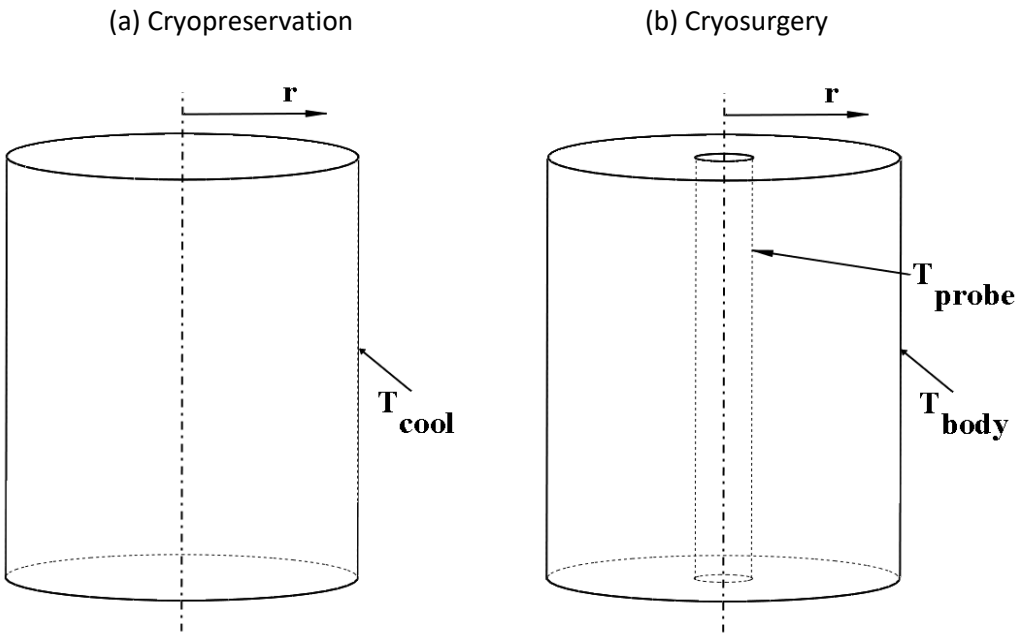

Figure 10. Geometry in Cylindrical Co-ordinates
Figure 9 has been reproduced from
(Bischof and Han 2002) and permission has been requested.

Cryopreservation involves cooling the system to temperatures < -80°C whereas cryosurgery freezes the system to a particular size so that unwanted tissue is killed. Following are the figures showing temperature history and phase front propagation for both applications. Each application

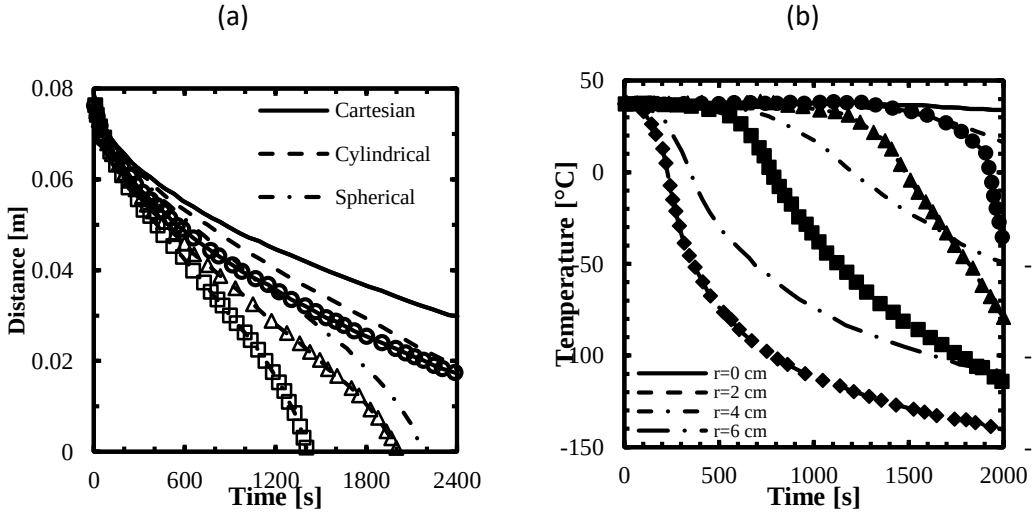

Figure 9. Numerical Simulation for Cryopreservation
(a) Phase Front Propagation (b) Thermal history for a cylinder
(Lines with symbols denote temperature dependent properties).
Figures 10 (a) and b have been reproduced from
(Bischof and Han 2002) and permission has been requested.

considers a planar, cylindrical and spherical system for a thickness or diameter of 8 cm. For cryopreservation, an initial condition of body temperature (37 °C) is considered over the solution domain. A temperature boundary condition of -160°C is applied at the surface with a symmetric boundary condition at the center. As seen in Figure 10, the phase front propagation is the fastest for the sphere and lowest for the cartesian system. Further, the temperature dependent boundary conditions speed up the ice-zone propagation, which in turn affects the temperature history as shown below.

In the case of cryosurgery, a temperature boundary condition of -160°C (applied by a cryoprobe) is considered at a radius of 1.5 mm for the radial systems or at one of the surfaces (0 mm) for the cartesian system. The second boundary condition considers a domain large enough to assume semi-infinite conditions (assuming the system is at body temperature). The same thermal properties as cryopreservation are used in this analysis. As seen from the results in Figure 11, the phase front propagates fastest for the cartesian system and slowest for the sphere. As seen before, this propagation is faster when temperature dependent properties are used. The interested reader may refer to (Bischof and Han 2002) for more information regarding this analysis.

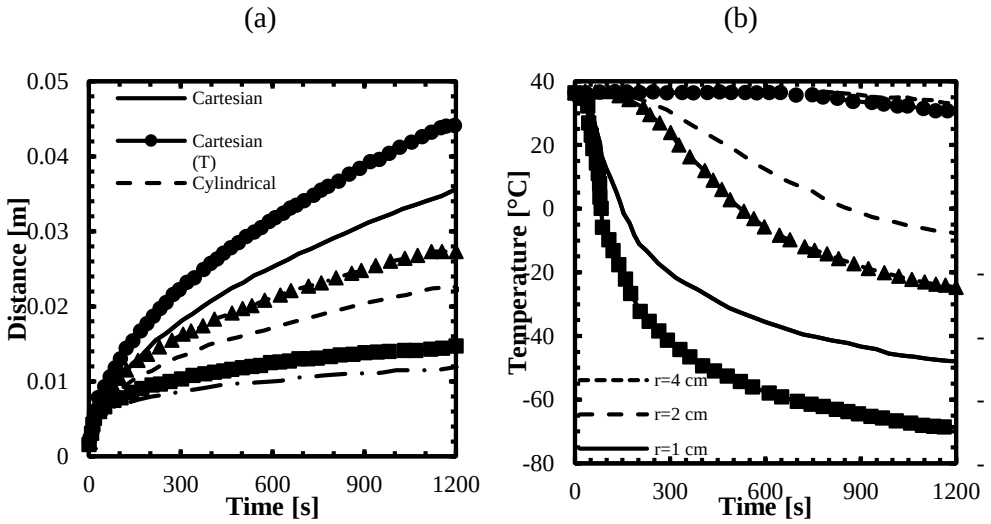

Figure 11. Numerical Simulation for Cryosurgery
(a) Phase Front Propagation (b) Thermal history for a cylinder
(Lines with symbols denote temperature dependent properties).
Figures 11 (a) and b have been reproduced from
(Bischof and Han 2002) and permission has been requested.

1.5 Conclusion

The goal of this review was to compile thermal conductivity and specific heat capacity values of human and porcine systems in the subzero and suprazero temperature ranges for the purposes of aiding the development of accurate models of conditions and pathologic treatments involving bioheat transfer mechanisms. As seen in data tables provided in the appendix, extensive datasets were available for thermal conductivity in both temperature ranges for porcine systems. However, limited data is available for both thermal conductivity and specific heat capacity for human systems in the subzero temperature range. Another area where there is limited data available is the effect of cryoprotectants on biomaterials. As was seen in Figures 5 and 6 for porcine liver, thermal properties of biomaterials are affected by the presence of cryoprotectants due to the presence of a vitreous or amorphous phase in addition to crystallization. Future thermal property measurements can be conducted by incorporating these changes to get a more accurate behavior to be applied in a model. As seen in the modeling case studies section, the importance of temperature dependent properties versus constant properties is reflected from the significant differences in the thermal histories for planar, cylindrical and spherical systems using water properties. Similar analyses can be performed by considering thermal properties of other biomaterials presented in this chapter.

Chapter 2: DSC Measurements of Cryoprotectants (CPAs)

2.1 Introduction

As discussed briefly in Chapter 1, cryopreservation techniques are important to achieve successful organ banking. The basic principle of cryopreservation involves in cooling the biomaterial to very low temperatures (< -80°C) in order to arrest biological activity. (Karlsson and Toner 1996). An important challenge to the success of cryopreservation is ice formation (or crystallization) which is fatal to the biomaterial. This challenge of controlling crystallization can be addressed by the use of cryoprotectants (CPAs). These CPAs increase the solute concentration in the biomaterial and thus reduce ice formation.

Broadly, there are two types of cryopreservation techniques, viz., conventional cryopreservation and vitrification. Conventional cryopreservation involves cooling at slow rates and aims to limit or avoid intracellular ice formation. (Mazur 1984). This technique allows for ice formation in the extracellular region and is applicable to small systems such as cells. In case of larger systems such as tissues and organs, extracellular ice formation needs to be avoided to maintain structural integrity of these systems (Song et al. 2000; Taylor et al. 2004). For larger systems, vitrification can be applied for successful preservation. Vitrification (glass formation) is a technique where in the biomaterial is cooled rapidly in the presence of high concentration CPAs to temperatures below -100°C to form a glassy phase (characterized by a high viscosity ~ 10^{13} poises) in order to avoid ice formation. (Fahy et al. 1984; Fahy et al. 2004). Some challenges for vitrification include the high cooling/warming rates required to avoid crystallization, the toxicity of CPAs due to high concentration, thermal stress effects and also heat transfer limitations based on the size of the system, i.e. cooling/warming rates are limited by increasing size of the system that is to be preserved.

Cryoprotectants (CPAs) are chemicals which are added to biomaterials to protect against the damaging effects of ice formation. Some examples include glycerol, dimethyl sulfoxide (DMSO) and sucrose. There are two types of CPAs, viz., penetrating and non-penetrating. Penetrating CPAs comprise of small molecules which penetrate into cells across the membrane. These CPAs reduce the amount of water in the cells and thereby reduce intracellular ice formation. Some examples include glycerol and DMSO. Non-penetrating CPAs comprising of larger molecules do not enter the cell and thus remove water from the cells due to osmotic difference. Some examples include sucrose and trehalose. In addition, compounds called as synthetic ice modulators

(SIM's)(Ehrlich et al. 2016), ice blockers ((Fahy et al. 2004) can also be used in order to inhibit or block ice nucleation and growth. CPAs used for studying vitrification (vitrification solutions) are usually a combination of these types of individual CPAs.

In the temperature domain of cryopreservation (-150°C to 37°C), there are three phases that are encountered: liquid, ice and glassy/vitreous phases. These phases are characterized by their corresponding temperatures which are explained in Figure 12, the phase diagram for glycerol in water. 'T_m' is the equilibrium melt/freezing temperature. When a CPA is cooled below T_m, it can crystallize heterogeneously at a temperature between T_m and T_h. 'T_h' is the homogenous nucleation temperature. Homogenous nucleation temperature is the temperature at or below which spontaneous ice nucleation is possible. 'T_g' is called as the glass transition temperature. This is the temperature at which the liquid state is converted to glassy/vitreous state. Lastly 'T_d' is called as the devitrification temperature. This is the temperature at which crystallization can happen while warming a CPA from lower temperatures.

For a given concentration, the temperatures between A and B and between B & C need to be

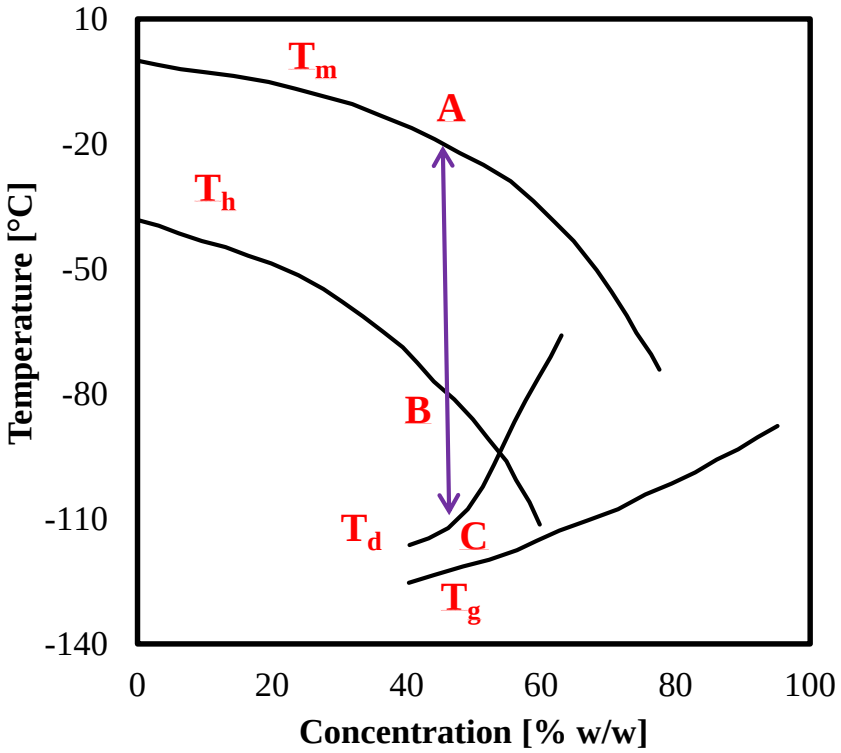

Figure 12. Phase Diagram of Glycerol in Water
Adapted from (Fahy et al. 2004)

bypassed quickly while cooling to prevent heterogeneous and homogeneous ice nucleation respectively. Similarly, the temperatures between C and A need to be bypassed quickly to prevent devitrification (crystallization while warming) while warming. These cooling and warming rates that are needed to avoid crystallization are called as Critical Cooling Rate (CCR) and Critical Warming Rate (CWR) respectively.

As discussed previously in Chapter 1, heat transfer models are helpful in predicting the thermal history as well as the cooling/heating rates encountered during a cryopreservation protocol. These cooling/heating rates can then be compared to the CCR and CWR of a particular CPA to predict the possibility of crystallization. For solving heat transfer models, thermal properties such as thermal conductivity, specific heat capacity and density need to be measured.

The general trends of thermal conductivity ('k') for various CPAs were discussed in Chapter 1. It was observed that there was little variation in the values of 'k' with temperature for higher concentrations (≥6M) of CPAs over the three phases, i.e. liquid, ice and glassy phases.

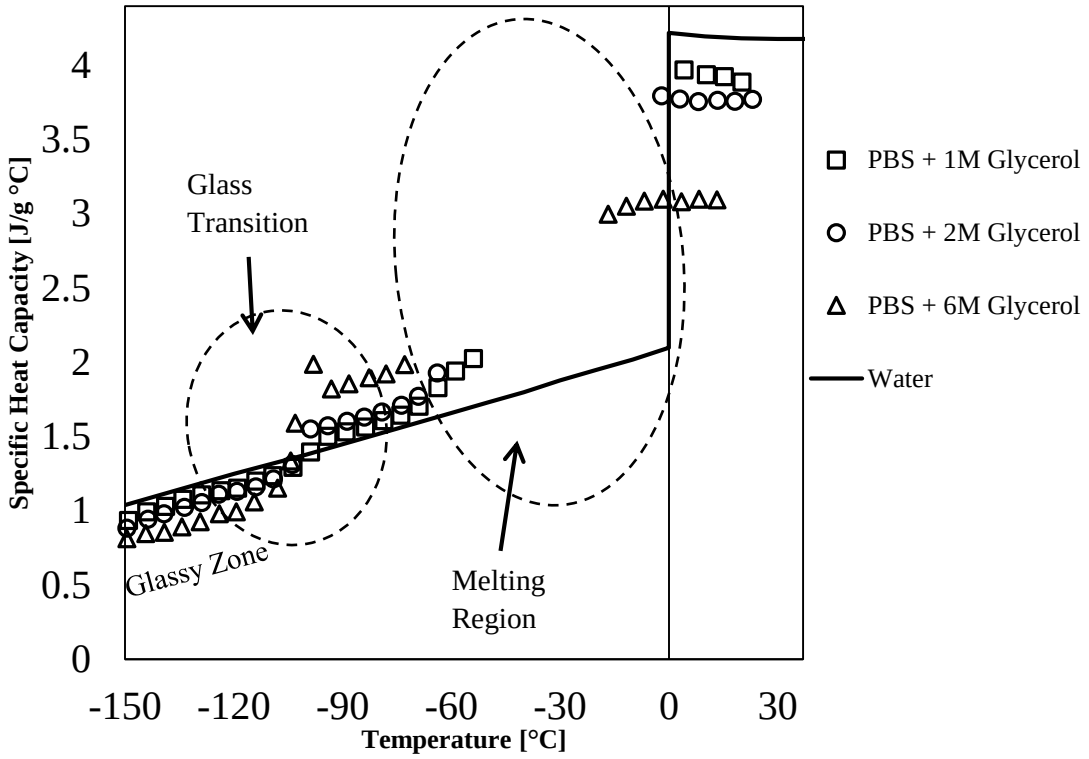

Figure 13. Specific Heat Capacity (c_p) for varying concentrations of glycerol

In the case of specific heat capacity (c_p), there is more variation in the values over the three phases. Figure 13 above shows the literature data for c_p of varying concentrations of glycerol Adapted from (Choi and Bischof 2008b).

As seen in Figure 13, the c_p is lowest for the glassy phase, followed by ice, liquid CPA and finally water has the highest c_p. Also experimental data is not directly available for the melting region due to the evolution of latent heat. The baseline c_p can be extracted from the evolution of latent heat which will be discussed in the results section of this chapter.

In addition to glycerol, data for thermal properties of various other vitrification solutions is not available. Table 3 indicates the current availability of these properties.

Table 3. Current Availability of Data for CPAs

Cryoprotectant	Thermal Conductivity	Specific Heat Capacity
Glycerol (6M)	(Choi and Bischof 2008b)	
DP6 (6M)	(Ehrlich et al. 2016)	Measured as part of this project
VS55 (8.4M)	NA	
M22 (9.345M)	NA	
VS55(8.4M) + 0.6M Sucrose	NA	
DP6(8.4M) + 0.6M Sucrose	NA	

The focus of this chapter is to provide the c_p as a function of temperature (-150°C to 37°C) for the CPAs listed in the table using a technique called as Differential Scanning Calorimetry (DSC). In addition, the crystallization behavior of CPAs for maximal, minimal and intermediate crystallization conditions has been measured. Specifically, crystallization behavior at 1, 5 and 10°C/min has been studied for all CPAs.

2.2 Materials and Methods

2.2.1 CPA Solutions

The CPAs studied as part of this project include VS55, DP6, M22, VS55+0.6M Sucrose and DP6+0.6M Sucrose. The composition of each of these CPAs are as follows:

VS55 (8.4 M) consists of 3.1 M DMSO, 2.2 M Propylene glycol, 3.1 M Formamide in a EuroCollins (EC) solution (Brockbank et al. 2015). DP6 (6 M) consists of 3 M DMSO and 3 M Propylene glycol in a EuroCollins (EC) solution. (Brockbank et al. 2015). These two solutions are similar except that Formamide is not present in DP6. M22 (9.345 M) consists of 2.855 M DMSO, 2.855M Formamide, 2.713 M Ethylene Glycol, 0.508 M N-Methylformamide, 0.377 M 3-Methoxy, 1,2-propanediol, PVP K12 (0.0056 M), PVA (0.005 M), PGL (0.0267 M) in a carrier LM5 solution (Fahy et al. 2004) where PVA and PGL are ice-blockers. VS55 + 0.6 M Sucrose and DP6 + 0.6 M Sucrose as the names suggest consist of VS55 and DP6 respectively in addition to 0.6 M sucrose added to each solution.

2.2.2 Differential Scanning Calorimetry (DSC)

Differential Scanning Calorimetry (DSC) was used to measure the specific heat capacity (c_p) of CPAs and also to study their crystallization behavior at 1,5 and 10°C/min. As explained in Chapter 1, DSC involves the measurement of the change of the difference in the heat flow rate to the sample and a reference while they are subjected to a controlled temperature program (Höhne et al. 1996). A simple schematic of the heat flux DSC is provided in Figure 14. below. As shown, it consists of a single furnace area where in the sample and reference pans are loaded. The temperatures are measured with thermocouples as indicated. The subsequent heat flow is proportional to the temperature difference between the sample and reference pans. Specific heat Capacity can be calculated by the following formula:

$$c_p = \frac{1}{m}\frac{d\emptyset_{sample}}{dt}\cdot\frac{dt}{dT}$$

A heat flux type DSC (TA Instruments Q1000) was used for all the measurements. The calibration steps as mentioned in Chapter 1 include baseline calibration, temperature calibration and heat flow calibration. The temperature calibration was performed using the transition temperatures of two known references: Indium (156.6°C) and Cyclohexane (-87.06°C and 6.54°C) while heat flow calibration was performed using Indium (28.47 J/g) for warming rates of 1,5 and 10 °C/min. An empty aluminum pan was used as a reference pan whereas CPA samples in the range 7-10 µL were loaded into the sample aluminum pan.

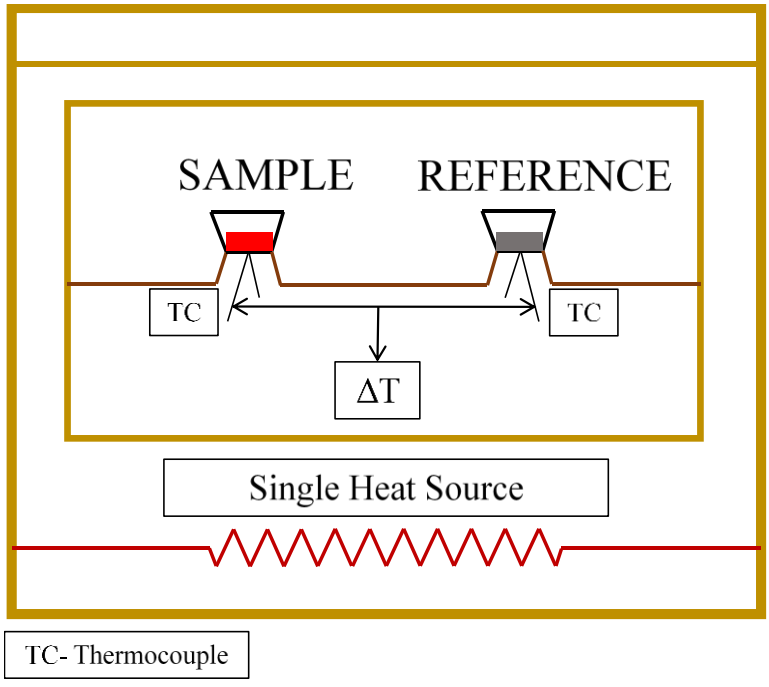

Figure 14. Schematic of a Heat Flux type DSC

Both pans were crimped before being loaded into the DSC.

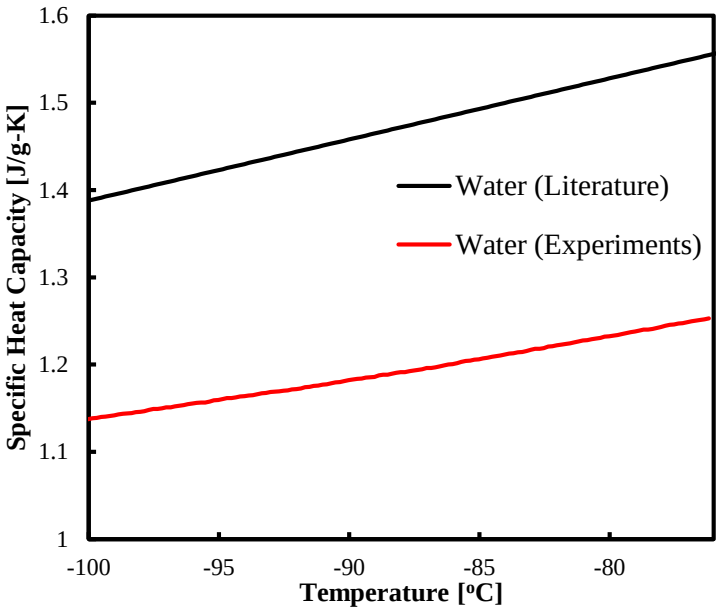

Figure 15. Slope differences between literature and experimental Cp of Water

Specific heat capacity measurements were always carried out while warming (Choi and Bischof 2008b) at rates of 5 or 10°C/min. For all c_p measurements, a temperature dependent normalization factor was multiplied to all c_p values of CPAs. This normalization factor was calculated every day as the ratio of literature c_p value of water to the measured c_p of water at all temperatures. The protocols used for water measurements were identical to those used for CPA measurements. This factor was used in order to correct for the slight day to day variations in the slopes as well as an offset between the measured c_p of water with respect to that of literature values. This variation for one instance is depicted in Figure 15.

As discussed previously, since crystallization is an important challenge that impedes successful cryopreservation, the c_p of CPAs was measured for two conditions: maximal crystallization and minimal crystallization. These two conditions show the limits of crystallization behavior of CPAs during a cryopreservation protocol. Minimal crystallization condition measurements are relevant to vitrification studies, i.e. rapid cooling to avoid crystallization. The thermograms (Heat Flow Vs Temperature plots) for these conditions and their corresponding protocols are discussed below.

The protocol for maximal crystallization was adapted from (Choi and Bischof 2008b). It involves the following steps: nucleation of the sample by initially super cooling from room temperature, reheating to the melt temperature and holding at this temperature for 3.5 mins, cooling down to -

150°C (start temperature for measurements) and finally a warming up step to measure c_p. Figure 16 depicts these steps for DP6. The detailed thermogram involving the steps for prenucleation and hold near the melt temperature can be found in the appendix. Figure 16 starts from the state

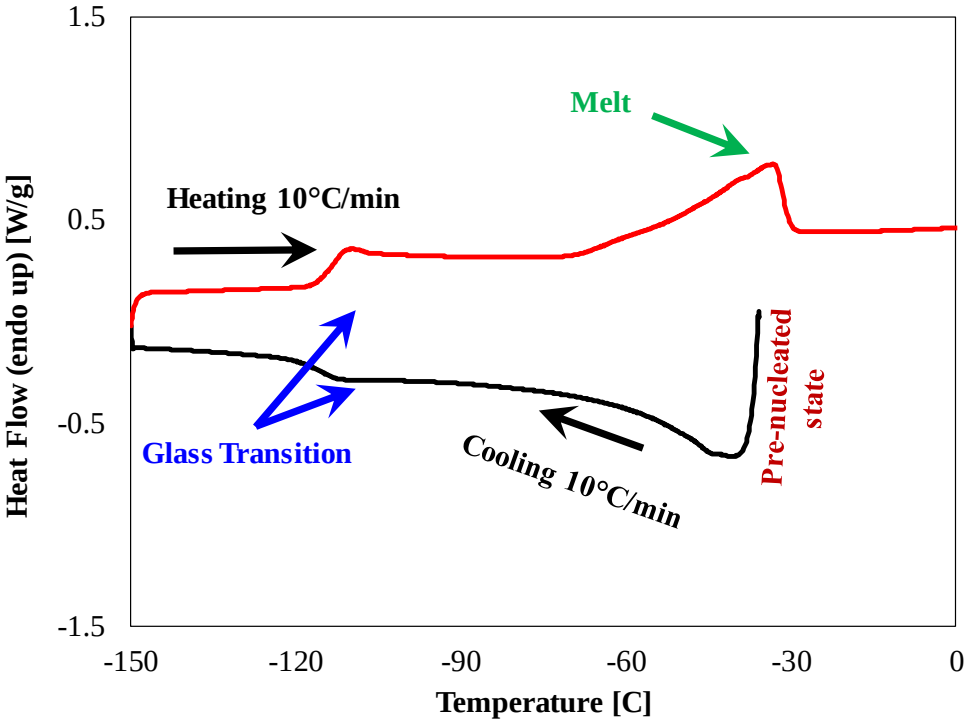

Figure 16. Thermogram for maximal crystallization

after the prenucleation and hold process had completed. Crystallization is associated with two steps, viz., nucleation and crystal growth. Nucleation was brought about by super cooling and hold near the melt temperature as mentioned above while crystal growth happened as the CPA was cooled to lower temperatures. These steps allowed for the CPA to be in a maximally crystallized state when it was cooled to -150°C. Another feature seen in Figure 16 that proves that maximal crystallization had occurred while cooling is the absence of any downward de-vitrification (crystallization while warming) peak during the warming step in spite of the warming rate (10°C/min) being less than the critical warming rate for DP6 (~200°C/min)(Rabin et al. 2005). As mentioned before, c_p was measured during warming. Also the c_p in the melting region above was not directly measured using the DSC due to evolution of latent heat as seen above. An extrapolation method (Choi and Bischof 2008b) involving the heat absorption ratio (i.e. ratio of latent heat evolved per degree at each temperature divided by the total latent heat) was used in order to calculate the c_p in this region. This method will be discussed in the results section.

The minimal crystallization condition is associated with having the CPA in a vitrified state at the start of the warming step for c_p measurement. This can be achieved by cooling the CPA at a rate greater than its critical cooling rate. An example thermogram for DP6 is shown in Figure 17. As seen, there is no crystallization during cooling. However, a devitrification peak (downward) is observed during warming as the warming rate is less than the critical warming rate of DP6. A warming rate of 10°C/min was maintained for the purpose of c_p measurements. The DSC has an inherent limitation to scan at higher warming due to instability issues. For the purpose of c_p measurements, data was recorded from -150°C to before the onset of the devitrification peak. Further c_p data was recorded between the post melt phase until 0°C. The data gap between start of devitrification and end of melting was fitted by a straight line with the assumption of vitrified conditions (i.e. no crystallization). These details will be provided in the results section.

In the case of both maximal and minimal modes of measurements, c_p data between 0-37 °C was extrapolated as a straight line as the DSC was not stable at temperatures above 0°C.

Lastly, an intermediate crystallization case is presented. This method simply involves cooling at

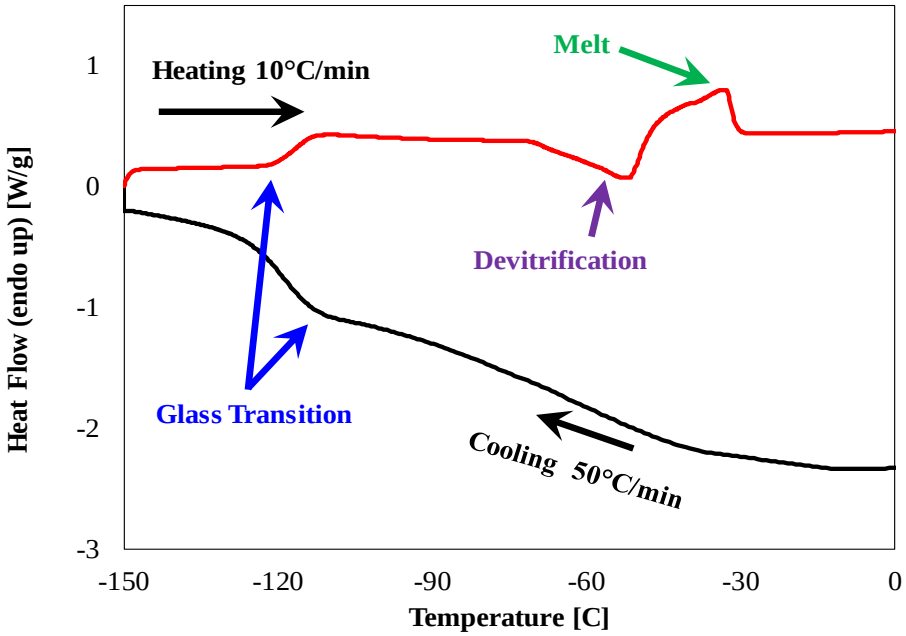

Figure 17. Thermogram for minimal crystallization

10°C/min and subsequent warming at 10°C/min. This is a non-prenucleated case of measurement. As seen in Figure 18 for 6 M Glycerol, a crystallization peak is observed during cooling as the cooling rate is less than the critical cooling rate of 6M glycerol (85°C/min). Similarly, a

devitrification peak is observed while warming as the warming rate is less than the critical warming rate of glycerol ($3.2*10^4$ C/min).

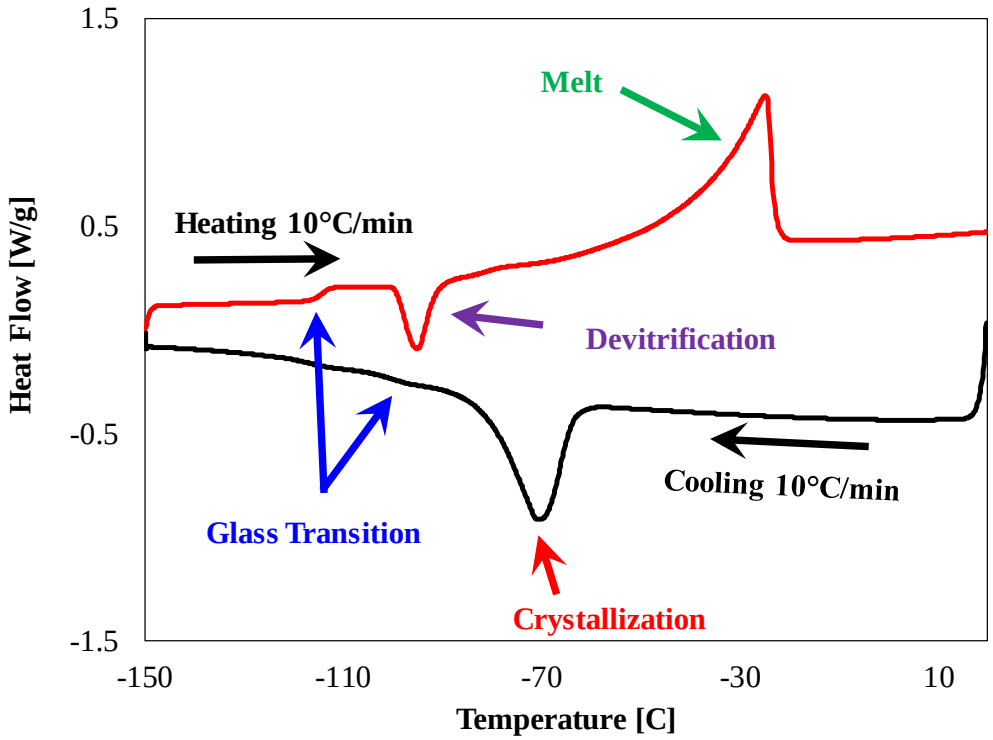

Figure 18. Thermogram for intermediate crystallization

Finally, crystallization effects at 1, 5 and 10°C/min are studied for all CPAs. The protocol followed here is simple a cool-heat cycle at each of the three rates to detect crystallization or devitrification and get an estimate of the critical rates.

2.3 Results and Discussion

Table 4 lists various thermal parameters of all the CPAs that have been studied. As seen in this table, 6M glycerol has the poorest thermal behavior owing to very high critical cooling and warming rates. DP6 (6M) in comparison having the same concentration has relatively lower CCR and CWR when compared to 6M Glycerol. The CCR and CWR for VS55 (8.4M) are even lower due to increase in concentration. In case of M22 (9.345M), the critical cooling and warming rates are very low which can allow for using slow rates for cooling and warming without the problem of crystallization. Lastly, VS55 and DP6 with added 0.6 M sucrose were studied in the DSC at rates 1, 5 and 10 °C/min.

However, these did not exhibit any crystallization effects while cooling and warming for all the three rates studied. The thermograms and c_p data for these CPAs is provided below:

Table 4. Thermal parameters of CPAs

CPAs	Glycerol (6M)	DP6 (6M)	VS55 (8.4M)	DP6 (6M) + Sucrose (0.6M)	VS55(8.4M) + Sucrose (0.6M)	M22 (9.345M)
Melting Point [^{0}C]	-26.3 ± 0.8 [3]	-34.7± 0.09	-43±0.4	NA	NA	-55 [2]
Latent Heat [J/g]	47.1 ± 3.5 [3]	42.5±0.7	24.6±0.7	NA	NA	NA
Glass Transition [^{0}C] (Approx.)	-100 [3]	-119	-123 [1]	-112	-115	-125
Critical Cooling Rate [^{0}C/min]	-85 [1]	-40 [4]	-2.5 [1]	NA	NA	0.1 [2]
Critical Warming Rate [^{0}C/min]	3.2*10^ 4 [1]	200 [4]	50 [1]	NA	NA	0.4 [2]

[1]: (Etheridge et al. 2014), [2]: (Wowk and Fahy 2005)
[3]: (Choi and Bischof 2008b) [4]: (Rabin et al. 2005)

The c_p data for all the CPAs is provided in Figures 19, 22 and 23. The c_p for VS55 and DP6 was

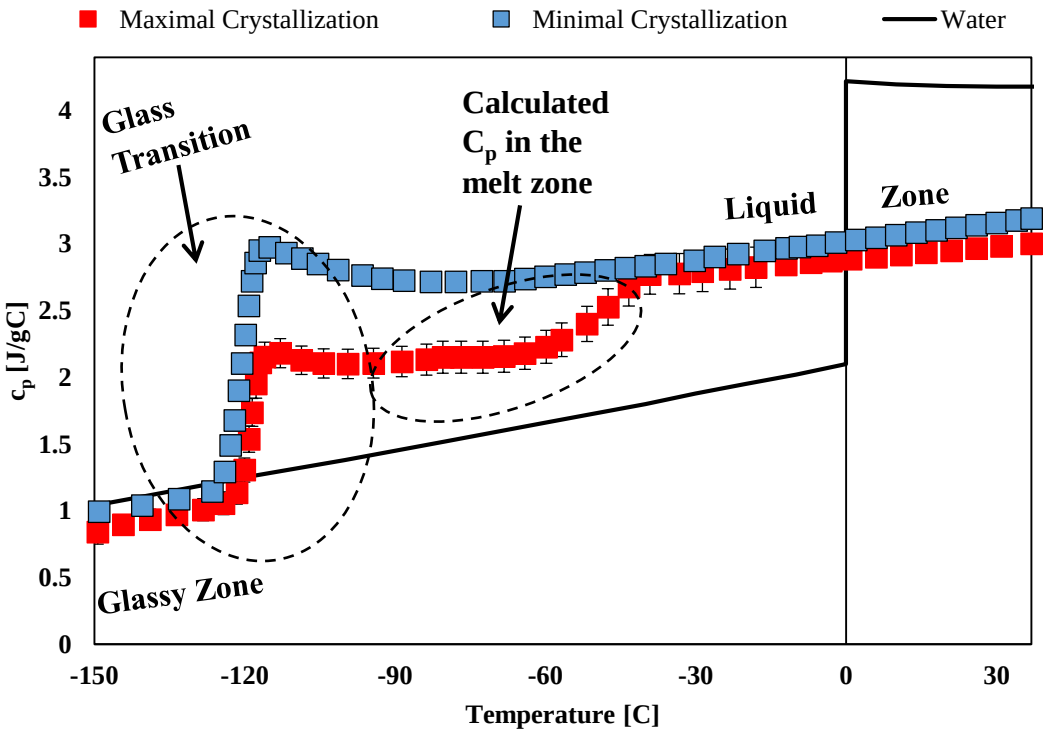

Figure 19. Specific Heat Capacity (c_p) of VS55 for maximal and minimal crystallization

measured in both the minimal and maximal crystallization modes. For the case of maximal crystallization, the calculation of c_p in the melting zone is also explained.

The behavior for both VS55 and DP6 is similar and hence only the data for VS55 is presented. The c_p data for DP6 is provided in the appendix. In case of M22, the critical cooling as well as

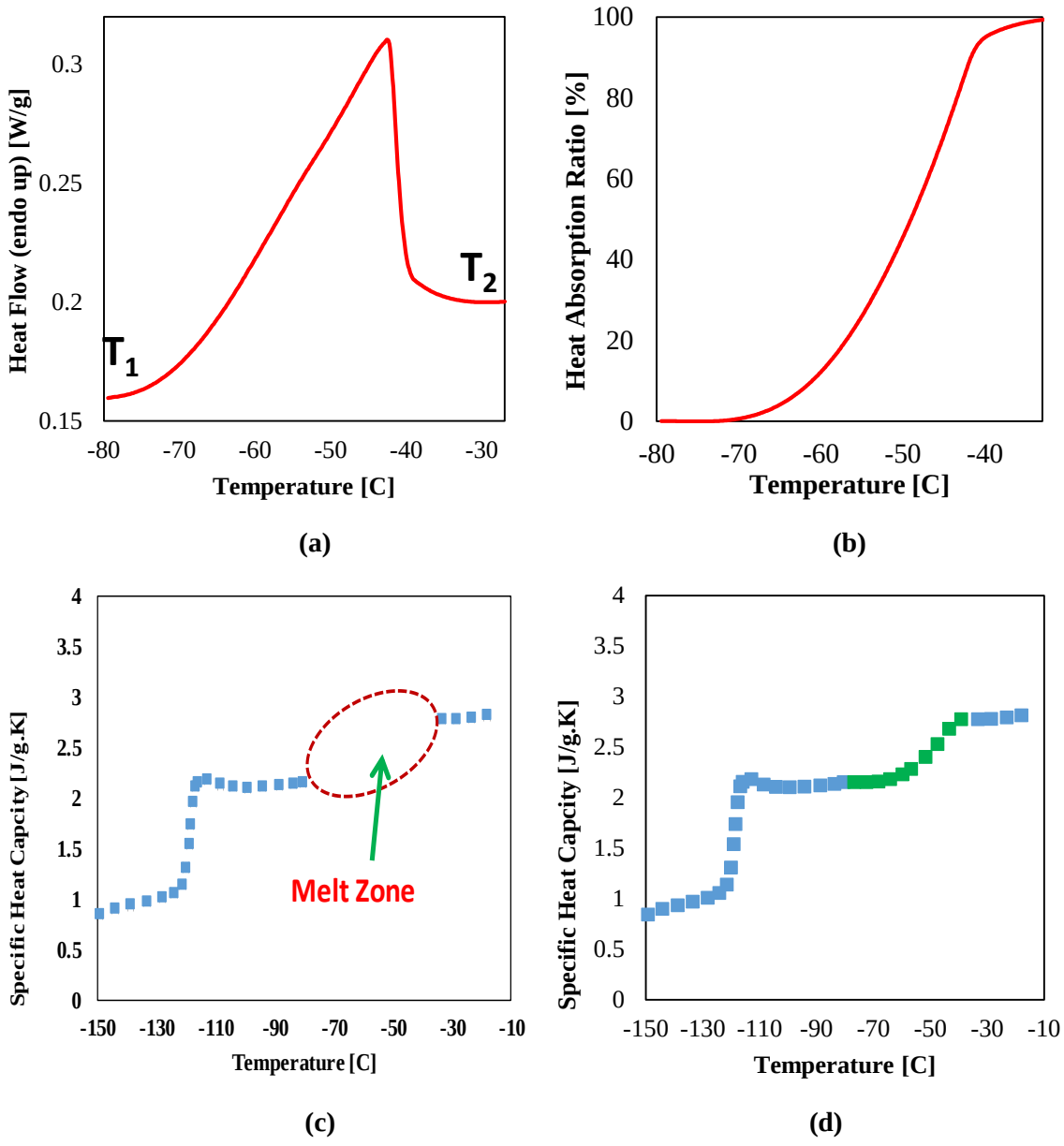

Figure 20. Calculation of Specific Heat Capacity (c_p) in the Melting Region
(a) Melting Region (b) Heat Absorption Ratio
(c) Melt Zone data region, (d) Calculated C_p in the Melt Zone

critical warming rates are very low as seen in Table 12. Hence the c_p data for M22 was measured simply by cooling at a fast rate and then heating at a rate of 10°C/min without any phase change

effects such as crystallization, devitrification and melting. As seen in Figure 19, the c_p of VS55 has been provided. The c_p data for water is plotted as well for comparison. For both minimal and maximal crystallization conditions, the glassy phase (around -150°C to -120°C) has the lowest c_p value followed by the c_p's of ice, liquid CPA and finally water having the highest c_p. Comparing between minimal vs maximal crystallization conditions, the c_p for minimal crystallization is almost equal to that of maximal crystallization in the glassy region (around -150°C to -120°C). Post glass transition, the c_p for minimal crystallization is consistently higher than that of maximal crystallization until the end of melting. This is due to larger amount of ice present in the maximal condition and that the C_p of ice being less than the liquid CPA phase. The c_p of the maximal condition increases as the melting process begins (around -70°C) and is equal to that of the minimal condition post melting as both are in the liquid phase. The calculation for c_p in the melting region (indicated by the dotted box) in Figure 20 is explained as follows:

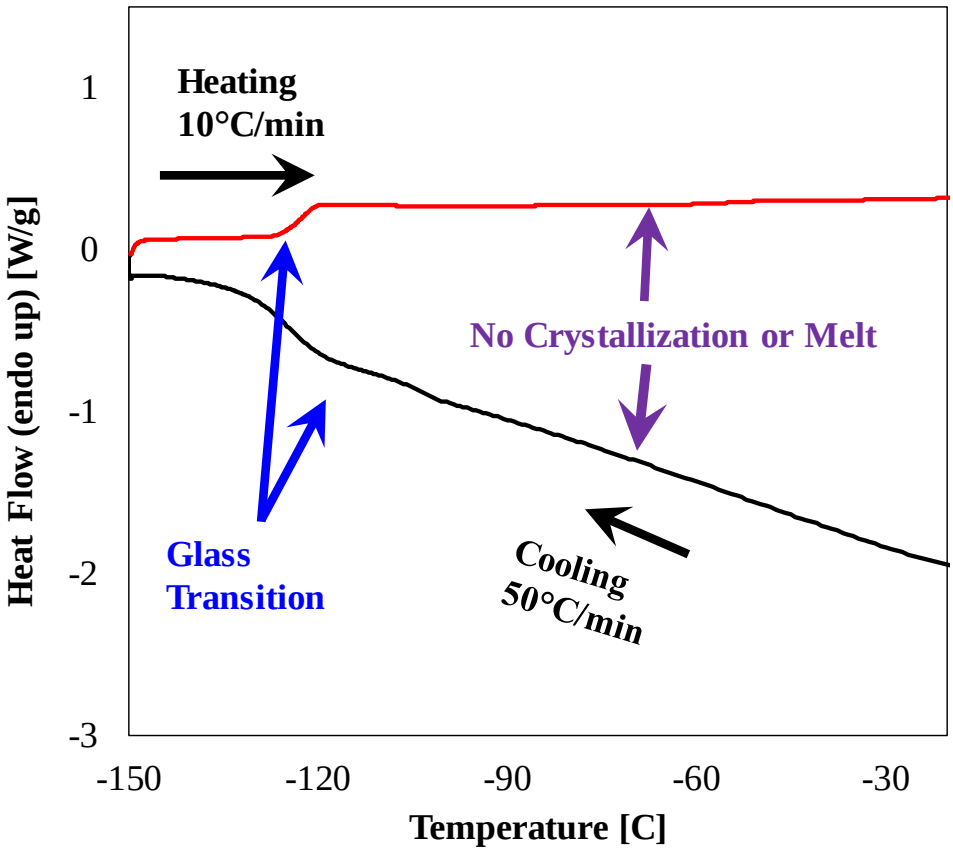

Figure 21. Thermogram for M22

The following formula was applied for calculation of the c_p in the melting region.

$$c_{p,\,melt\,zone}(T) = c_p(T_1) + HR(T) * \left[c_p(T_2) - c_p(T_1)\right] \quad for\ T_1 \leq T \leq T_2$$

Where c_p (T_1) is the specific heat capacity of the CPA before the melting region (~80°C in Figure 20 (a), above), c_p (T_2) is the specific heat capacity of the CPA post melting (~-30°C in Figure 20 (a), above) and HR (T) is called as the heat absorption ratio for the temperature region $T_1 \leq T \leq T_2$. It can be defined as the ratio of latent heat evolved per degree divided by the total latent heat evolved as part of the melting process. The latent heat is the area under the curve provided in Figure 20 (a) whereas the heat absorption ratio is plotted as a function of temperature in Fig 20 (b). As seen from Fig 20 (d), the c_p gradually increases through the melting process owing to gradually increasing liquid phase in the CPA.

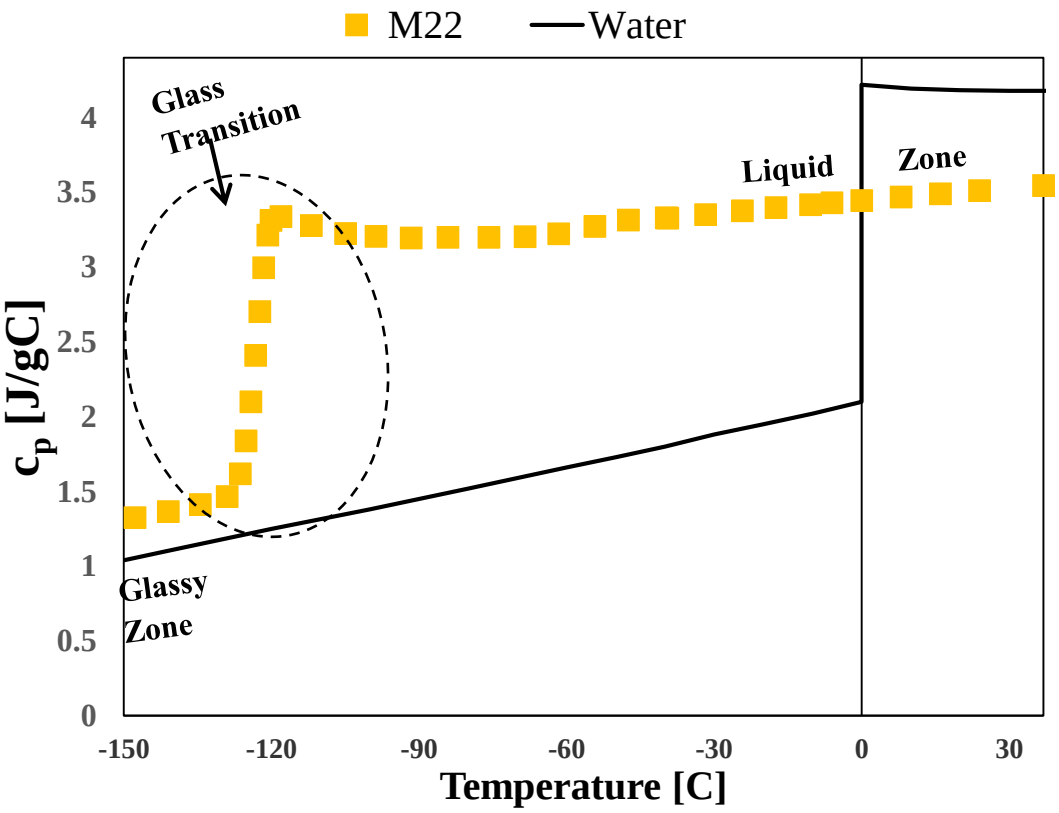

Figure 22. Specific Heat Capacity (c_p) of M22

In the case of M22, due to very low critical cooling and warming rates (Fahy et al. 2004), no crystallization or melting was observed as seen in the thermogram in Figure 21. M22 was designed to vitrify at lower rates such as 10°C/min, hence the case of maximal crystallization is not applicable. Considering c_p data for M22 in figure 22, the general behavior is similar to the other CPAs. The only difference is that the c_p of M22 is higher than ice in the glassy zone (around -150°C to -120°C) whereas it was slightly below that of ice for other CPAs in the glassy zone as seen in Figure 19. This higher c_p will lead to slightly lower cooling/warming rates as compared to other CPAs.

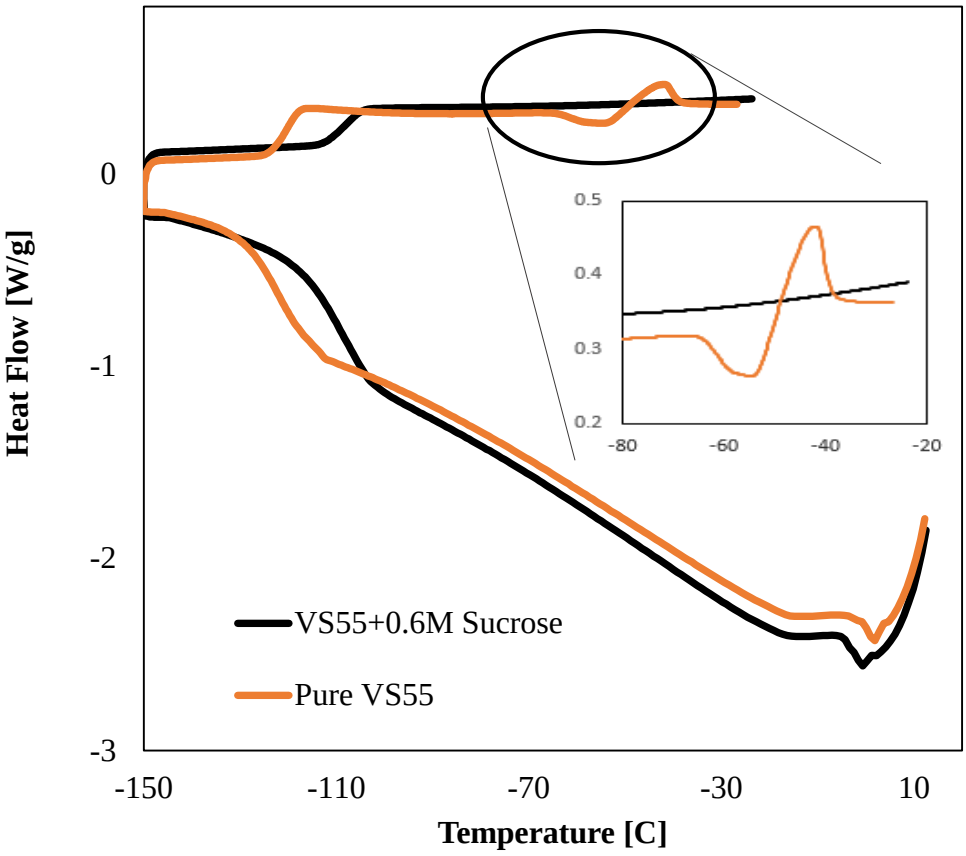

Figure 23. Thermogram for VS55 + 0.6 M Sucrose

Finally, VS55 and DP6 were studied with added 0.6 M sucrose. The thermogram is presented in Figure 23. The important part as seen is that addition of sucrose prevents any crystallization, devitrification or melting for both VS55 and DP6. The glass transition temperature increases on addition of sucrose by 8°C and 7°C for VS55 and DP6 respectively. There is significant reduction

in the CCR and CWR when sucrose is added when compared with pure VS55 (CCR: 2.5°C/min, CWR 50°C/min) or DP6 (CCR: 40°C/min, CWR 200°C/min) as can be seen from Table 4 above. VS55 and DP6 with 0.6 M sucrose were tested at cooling/warming rates of 10, 5 and 1°C/min.

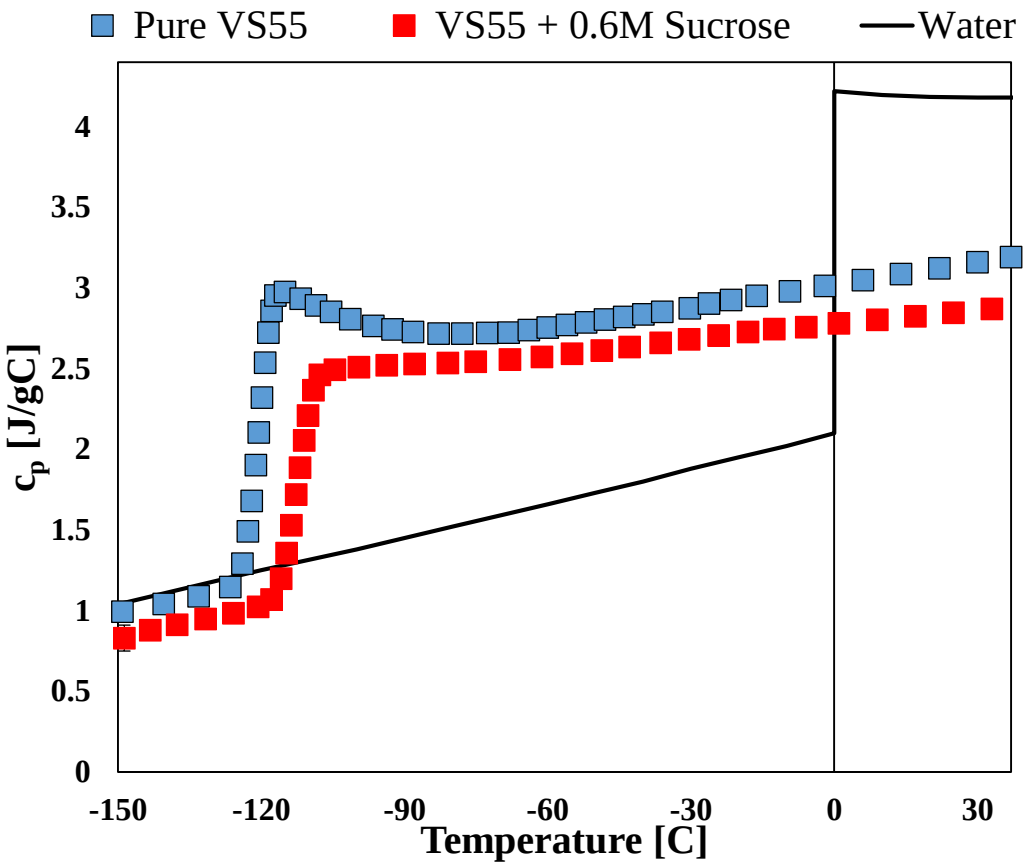

Figure 24. Specific Heat Capacity (c_p) of VS55 and VS55 + 0.6 M Sucrose

No crystallization or devitrification was observed for all three rates.

The c_p data characterized at 10°C/min for VS55 with 0.6 M sucrose is shown in Figure 24 along with pure VS55. The consistent trend seen is that addition of sucrose results in a slight decrease in the c_p compared to pure VS55. A similar behavior was seen for DP6 with 0.6 M sucrose and the corresponding c_p data has been provided in the appendix.

Critical Cooling and Warming Rates in Table 4 have been determined based on DSC studies where the volume size of the sample is of the order of microliters. As seen in (Fahy et al. 1990), absence of vitrification in small DSC samples did not directly relate to larger volumes. Ice nucleation was observed for volume sizes of ~50 ml and ~500 ml. Hence the CPAs with added sucrose should be studied in larger volumes to see any presence of crystallization.

This will help in validating the DSC results for all the three scanning rates as seen in Table 5. A similar study can be done in higher volumes for DP6 as well which did not crystallize while cooling at rates of 5 and 10°C/min as seen in Table 5. The critical cooling rate for DP6 based on DSC measurements has been reported to be 40°C/min in (Rabin et al. 2005).

Adding sugars raises the T_g (glass transition temperature) when compared to pure VS55 and DP6

Table 5. Crystallization Summary of CPAs

CPAs	Glycerol (6M)	DP6 (6M)	VS55 (8.4M)	DP6 (6M) + Sucrose (0.6M)	VS55(8.4 M) + Sucrose (0.6M)	M22 (9.345M)
Crystallization during cooling (no prenucleation)						
1 ^{0}C/min	NA	NA	NA	No	No	No
5 ^{0}C/min	Yes [3] (Partial)	No	No	No	No	No
10 ^{0}C/min	Yes (Partial)	No	No	No	No	No
Crystallization during warming (no prenucleation)						
1 ^{0}C/min	NA	NA	NA	No	No	No
5 ^{0}C/min	Yes [3] (Partial)	Yes	Yes	No	No	No
10 ^{0}C/min	Yes (Partial)	Yes	Yes	No	No	No

[1]: (Etheridge et al. 2014), [2]: (Wowk and Fahy 2005)
[3]: (Choi and Bischof 2008b) [4]: (Rabin et al. 2005)

as seen in Table 4 above. A similar behavior was observed by (Kuleshova et al. 1999) when sugars such as sucrose, trehalose and raffinose were added to ethylene glycol-saline solutions. Sutton (Sutton 1992) observed that the CCR and CWR of CPAs slightly dropped in presence of sugars. However as mentioned above, these studies should be performed in higher volumes as there are more chances of crystallization in larger systems. As seen in Table 4, the critical cooling and warming rates increase as the concentration of the CPA is reduced. In case of cryopreservation of small systems such as mouse oocytes (~120 µm) (Jin et al. 2014), the addition of sucrose to low concentration CPAs (1-4M) can be studied to see if the critical cooling and warming rates drop as dramatically as seen in the crystallization summary table above.

2.4 Conclusion

The DSC studies in this Chapter helped measure temperature dependent specific heat capacity of five CPAs. The specific heat capacity was measured in the minimal and maximal modes of crystallization for VS55 and DP6 to understand the limits of crystallization behavior. A maximal case is not applicable for M22 as it does not crystallize at practical cooling/heating rates. These thermal properties can be utilized in a thermal model to study the thermal history and hence cooling/warming rates as will be shown in Chapter 3. The addition of 0.6 M sucrose to VS55 and DP6 suppressed crystallization and devitrification at practical scanning rates (1, 5 and 10 °C/min). Further studies using cryomicroscopy as well as cooling/warming in higher volumes can be done for these CPAs to study the crystallization effects as mentioned in the section above. Another area that can be pursued is the measurement the c_p data for tissues perfused with these CPAs (Choi and Bischof 2008a) in the cryogenic regime. This can help in modeling these systems to correlate with their corresponding experimental cooling and heating measurements.

Chapter 3: Thermal Modeling of Cryoprotectants (CPAs) to study Vitrification

3.1 Introduction

The focus of this chapter is to perform a parametric heat transfer modeling study for a cylindrical geometry to calculate the cooling and warming rates experienced in a cylindrical geometry. As discussed in Chapter 2, the presence or absence of crystallization effects while cooling/warming for cryopreservation by vitrification is determined by the critical cooling and warming rates.

This modeling study consists three cases, viz. convective cooling, convective warming and nanowarming (volumetric warming). The cooling or heating of bio-materials is usually carried by boundary cooling or warming as was seen in Figures 10 and 11 in the modeling case study in Chapter 1 where a constant temperature boundary condition was applied at the outer surface. The problem with convective cooling or warming techniques is that these methods fail to exceed the critical cooling / warming rates as the geometry size increases. This is limited due to heat transfer principles and will be discussed in further sections. The geometry dimensions were chosen as seen in Table 6, where 'V' is the volume, 'D' is the diameter and 'H' is the height of the cylinder. These sizes were chosen considering the sizes of various human organs/ tissues that can be potentially stored in cylindrical containers of these sizes.

Table 6. Geometry Dimensions and Target Biomaterials for the Model

V [ml]	1	80	160	500	1300
D [cm]	1	3.5	5	7	12
H [cm]	1	8	8	13	12
Target Human Biomaterials	Ring / Valve Segments	Vessels, skin, heart valve, cartilage, ovaries, pancreas	Kidney, Intestine, Pancreas	Kidney, Hand/limb, Heart, Intestine	Liver, Heart, Hand/limb

Two scenarios were investigated using this model. Firstly, the size limitation of the cylinder geometry, i.e. the size beyond which the cooling rates would not be able to exceed the critical cooling rate was tested for all the three cases. In case of convective cooling, the effects of increasing values of the convective coefficient as well as the effects of changing the thermal properties, (i.e. across all the CPAs studied in Chapter 2) on the cooling rates were tested. As seen in Table 4 in Chapter 2, the critical warming rates are much higher than the critical cooling rates. As will be seen in subsequent sections in this Chapter, convective warming resulted in very

low values of warming rates which failed to exceed the critical warming rates of most CPAs studied due to very slow warming rates. Hence volumetric warming (i.e. nanowarming) was utilized to increase these warming rates. As shown in (Manuchehrabadi et al.; Etheridge et al. 2014) RF excited magnetic nano-particles (0.3 % v/v) were mixed with the CPA VS55 to achieve rapid warming rates and prevent devitrification while warming in cylindrical systems up to a volume of 80 ml. These nano-particles were excited by means of inductive coil heating. The second scenario tested was to see the effect of increasing power inputs to the inductive coil on the warming rates experienced in the cylinder. The goal was to find the minimum amount of power that was needed to successfully exceed the critical warming rate in all the cylinder sizes for all the CPAs that were studied in Chapter 2.

3.2 Methods

The model consists of a simple cylinder geometry. This geometry was modeled in COMSOL as a transient conduction heat transfer 2-D axisymmetric analysis. Phase change effects associated with ice formation were neglected as the goal was to study vitrification. The problem definitions and boundary conditions for convective cooling, convective warming and nano-warming are shown in figure 25 (a), (b) and (c) respectively. All cooling and warming rates were calculated at

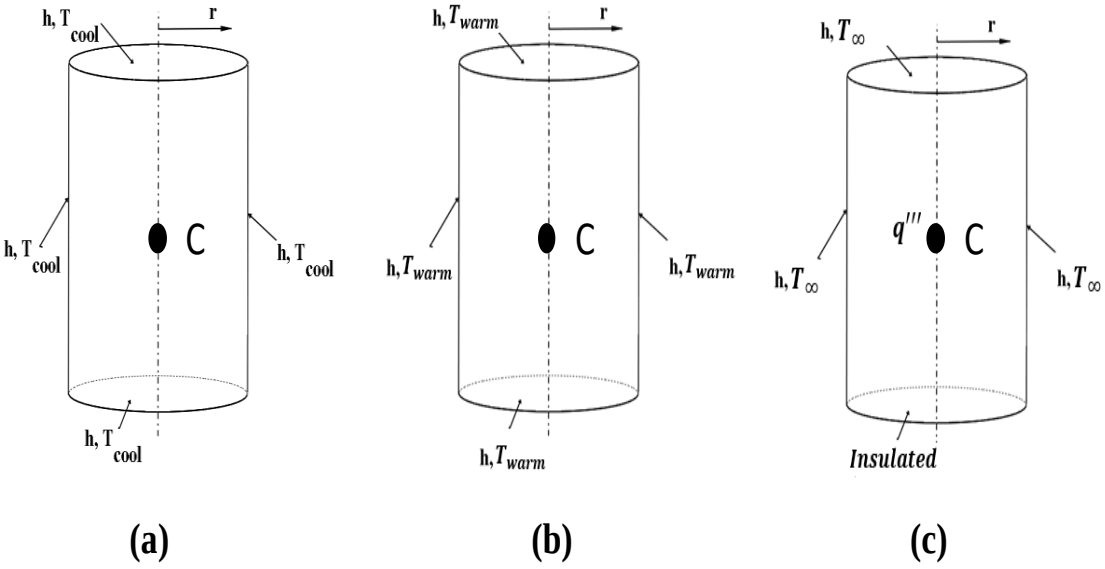

Figure 25. Problem Geometry and Boundary Conditions
(a) Convective Cooling, (b) Convective Warming
(c) Nano-Warming

the center of the cylinder (as indicated by the black dot) as it will exhibit the slowest cooling or warming rates. The necessary thermal properties include thermal conductivity (k), specific heat

capacity (c_p) and density (ρ). Thermal conductivity (k) was assumed to be constant (0.3 W/m-K) (Etheridge et al. 2014) due to less variation versus temperature as seen for high concentration cryoprotectants in Figure 7, Chapter 1. Temperature dependent specific heat capacity (c_p) of CPAs was utilized from the DSC measurements in Chapter 2. Finally, due to unavailability of data for density for all CPAs, the temperature dependent density of VS55 was assumed for all the studied CPAs as was used in (Etheridge et al. 2014).

The three modeling cases in terms of the values of boundary temperatures, heat transfer coefficients, initial temperatures and heat generation values (in case of nano-warming) are discussed as follows:

For convective cooling, an initial temperature of 0°C was applied along with a convective boundary condition at the surface where three values of heat transfer coefficients (h) were considered (15; 150 and 10,000 W/m^{2}K) with the surrounding temperature (T_{cool}) being -160°C. An 'h' of 15 W/m^{2}K was considered for a free convection in a cold air environment (Eisenberg et al. 2016), 'h' of 150 W/m^{2}K was considered to be a liquid N_2 vapor environment (Eisenberg et al. 2016) and an 'h' of 10,000 W/m^{2}K was considered to be in a boiling liquid N_2 environment (He et al. 2008).

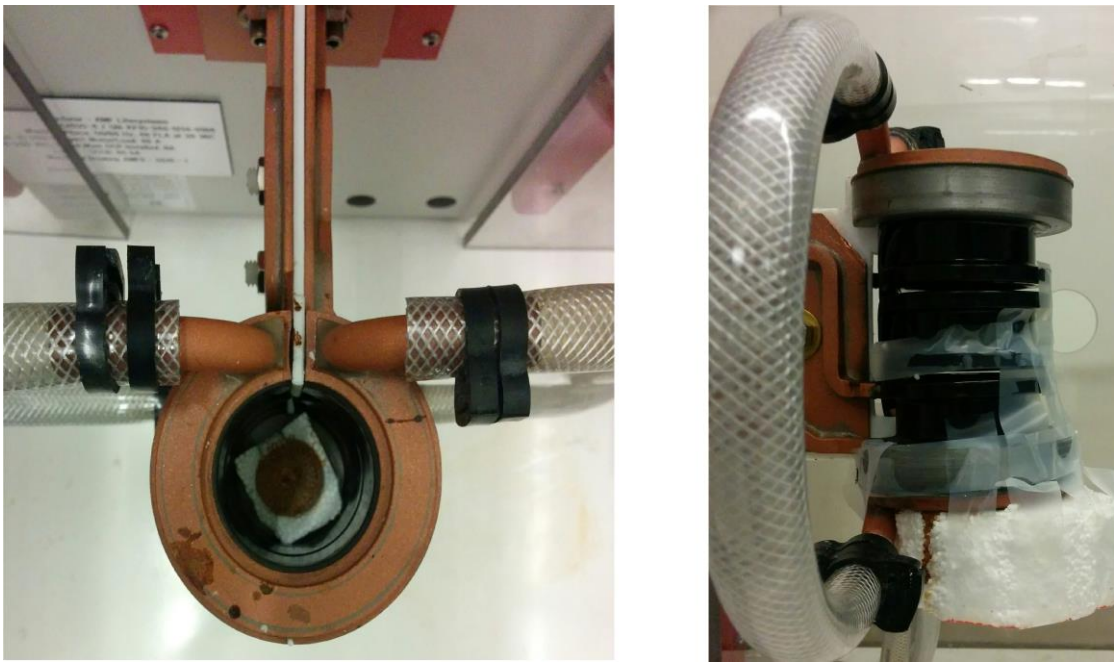

(a) **(b)**

Figure 26. Nano-Warming Coil (15 kW)
(a) Top View, (b) Side View

For convective warming, an initial temperature of -150°C was applied along with a convective boundary condition at the surface where a value of 25 W/m^2K was used for a hot water bath environment (Etheridge et al. 2014) at a temperature (T_{warm}) of 37°C.

For nano-warming, an initial temperature of -150°C was applied along with convective boundary conditions along the lateral surfaces and the top of the geometry where 'h' was 15 W/m^2K at room temperature of 20°C. The bottom surface was insulated by using styrofoam as seen in Figure 26 above. Finally, uniform heat generation was considered throughout the system geometry for all volumes. This heat generation can be brought about by low RF excitation (Alternating Magnetic Field) of magnetic nano-particles which are added to the CPA (Manuchehrabadi et al.; Etheridge et al. 2014). The heating of the cylinder geometry is carried out in the inductive coil for three values of power 1kW, 15 kW and 150 kW. This inductive coil used for nano-warming is shown in Figure 26. A volume size of 1 ml was heated in a 1 kW system, 80 and 160 ml in a 15 kW system and 500 ml and 1.3 L systems were heated in a 150 kW system. The heat generated by exciting the nano-particles is called as SAR (Specific Absorption Rate) which has the unit's W/ g of Fe. Heat generation (W/m^3) is the product of SAR and the concentration of nanoparticles dispersed in the CPA. The concentration of these nano-particles considered for the analysis was 10 mg Fe/ml. Two types of nano-particles were considered: commercially available magnetic iron oxide nano-particles, IONP (EMG308, Ferrotec) and meso-porous silica coated iron oxide nano-particles (msIONP). Table 7 displays the values of SAR and subsequent heat generation values for the three system sizes.

Table 7. SAR and Heat Generation Values

RF System [kW]	msIONP		EMG308	
	SAR [W/g Fe]	q'''* 10^6 [W/m^3]	SAR [W/g Fe]	q'''* 10^6 [W/m^3]
1	180	1.8	250	2.5
15	640	6.4	700	7
150	1800	18	2500	25

(Manuchehrabadi et al.)

For the case of nano-warming, thermal properties solely of CPAs were assumed for the mixture of CPAs and nano-particles. VS55 with added nano-particles (< 0.3 % v/v) was previously studied (Etheridge et al. 2014) to see negligible difference in the heat flow in the presence of nano-particles. In addition, as seen in (Xu et al. 2016), ice nucleation and crystal growth is seen to be less in the presence of nanoparticles in the CPA VS55 as compared to more number ice nucleating sites and subsequent crystal growth in pure VS55.

3.3 Results and Discussion

Convective cooling was tested for VS55, DP6, M22, VS55 + 0.6 M sucrose and DP6 + 0.6 M sucrose. The study was conducted for these CPAs for three values of the heat transfer coefficient across all the system sizes as shown in Table 8. The center line cooling rate between 0°C to

Table 8. Centre Cooling Rates for Convective Cooling

CPA	V [ml]	1	80	160	500	1300
	D [cm]	1	3.5	5	7	12
	h [W/m^{2}K]	Centre Cooling Rate [°C/min]				
VS55 [CCR: 2.5°C/min]	15	15	2.5	1.6	0.95	0.5
	150	70.6	6.4	3.5	1.79	0.8
	10000	117.6	8	4	2	0.83
DP6 [CCR: 40°C/min]	15	16	2.6	1.7	1.03	0.6
	150	74	7	3.8	1.94	0.9
	10000	128	8.6	4.3	2.18	0.91

-100°C was calculated by dividing the temperature interval (100°C) by the time required to reach that temperature. Table 8 provides the cooling rates for VS55 and DP6. As seen, VS55 shows cooling rates greater than the CCR up to a maximum system size of 160 ml whereas DP6 fails at volume sizes beyond 1 ml itself. For M22, VS55 and DP6 with 0.6 M sucrose, the cooling rates observed always exceeded the critical cooling rates of these CPAs. In the case of sucrose, the cooling rates always exceeded 1 °C/min for all sizes except the final size of 1300 ml. These results have been presented in the appendix.

As discussed in the introduction, the effect of increasing values of the heat transfer coefficient on the cooling rates was tested for convective cooling. Figure 27 shows such a plot for VS55 across all system sizes. As seen in the plot, there is no appreciable rise in the cooling rates obtained when the heat transfer coefficient is increased from 150 to 10,000 W/m^{2}K. This behavior is similar across all CPAs. Thus an 'h' of 150 which is associated with a forced convection environment in liquid N_2 vapors can be considered to be the limit to get the highest cooling rates possible in this case for convective cooling. The second part tested in case of convective cooling was to see the effect of different CPAs, i.e. change in the thermal properties on the cooling rates obtained. This is shown in Figure 28. As seen from the figure, beyond the smallest system size (1 cm in diameter), all the cooling rates are practically the same across all CPAs. Presence or absence of crystallization will be determined by the critical cooling rate. Thus the system dimensions and critical cooling rate are more critical parameters as compared to the thermal

properties of the system. M22 exhibits slightly lower cooling / warming rates due to its higher specific heat capacity.

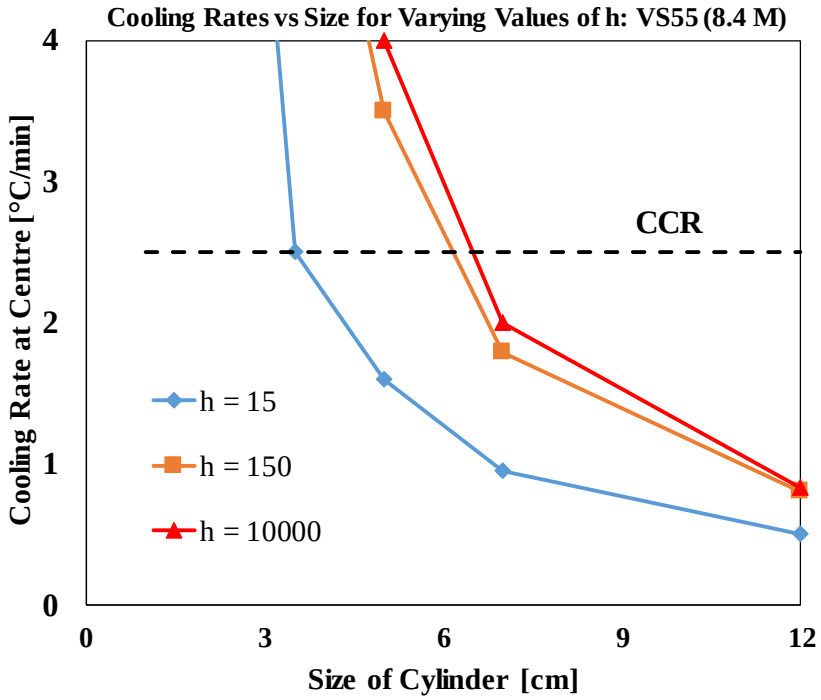

Figure 27. Effect of 'h' on cooling rates in VS55 for convective cooling

In case of convective warming, the centre warming rates have been provided in Table 9 for VS55, DP6 and M22. These warming rates were calculated for a temperature interval between -150°C and 0°C. The warming rates for VS55 and DP6 with added 0.6 M Sucrose were consistently higher than what was observed in the DSC. As seen in Table 9, M22 again was able to have higher rates than the CWR. The rates for VS55 and DP6 failed to exceed their respective CWR's for all the system sizes in case of convective warming.

Table 9. Centre Warming Rates for Convective Warming

CPA	V [ml]	1	80	160	500	1300
	D [cm]	1	3.5	5	7	12
	CWR [°C/min]	Centre Warming Rate [°C/min]				
VS55	50	23.7	3.5	2.2	1.26	0.7
DP6	200	24.7	3.7	2.4	1.36	0.6
M22	<1	20.2	3	1.9	1.1	0.6

In addition to very low warming rates with increasing volumes as seen in Table 9, convective warming leads to non-uniform heating and thus large thermal gradients as shown in Figure 29.

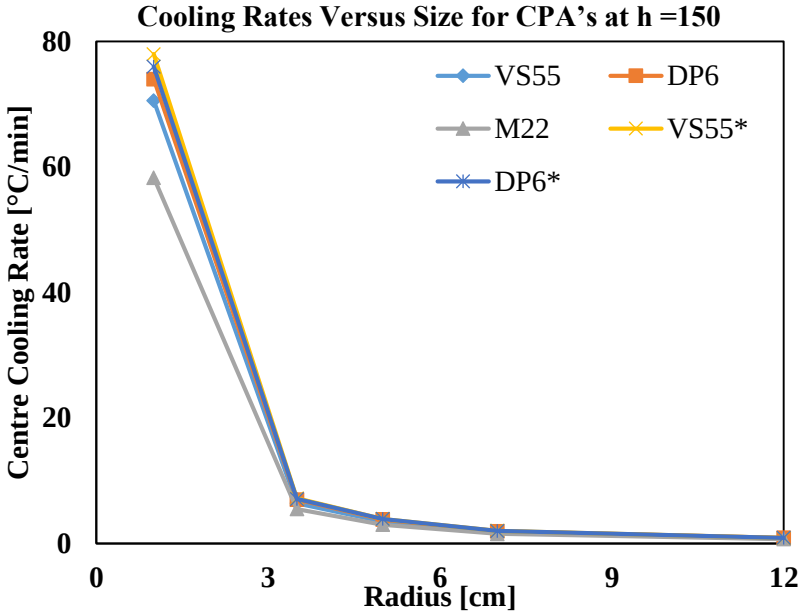

Figure 28. Effect of thermal properties on cooling rates during convective warming

Hence it was necessary to use a different technique which could achieve uniform and fast

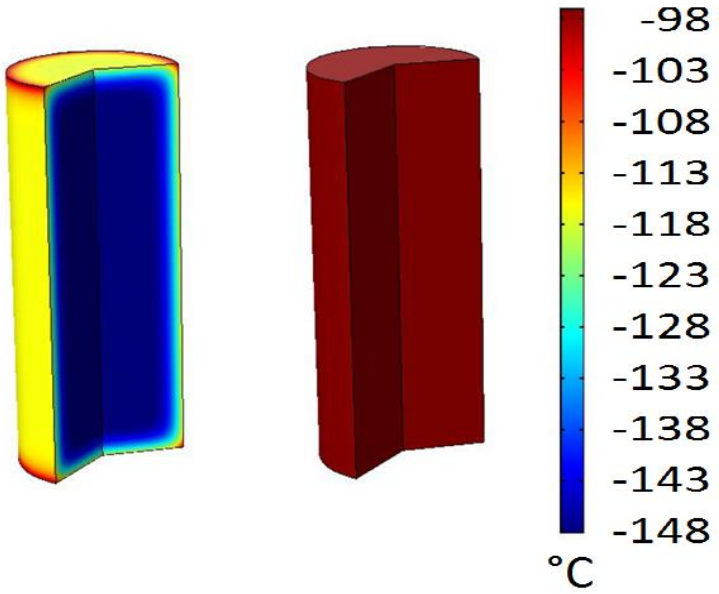

Figure 29. Convective Warming Vs Nano-Warming at a Time of 20 sec
Left: Convective Warming, Right: Nano- Warming

warming so as to exceed the critical warming rates for all the CPAs studied. This was achievable using nanowarming which provided uniform and fast heating. The second scenario investigated was to find the amount of power that was needed by the inductive coil to produce enough heat so as to exceed critical warming rates in the CPAs. Figure 30 shows such a plot of warming rates for two different powers across all system sizes for VS55.

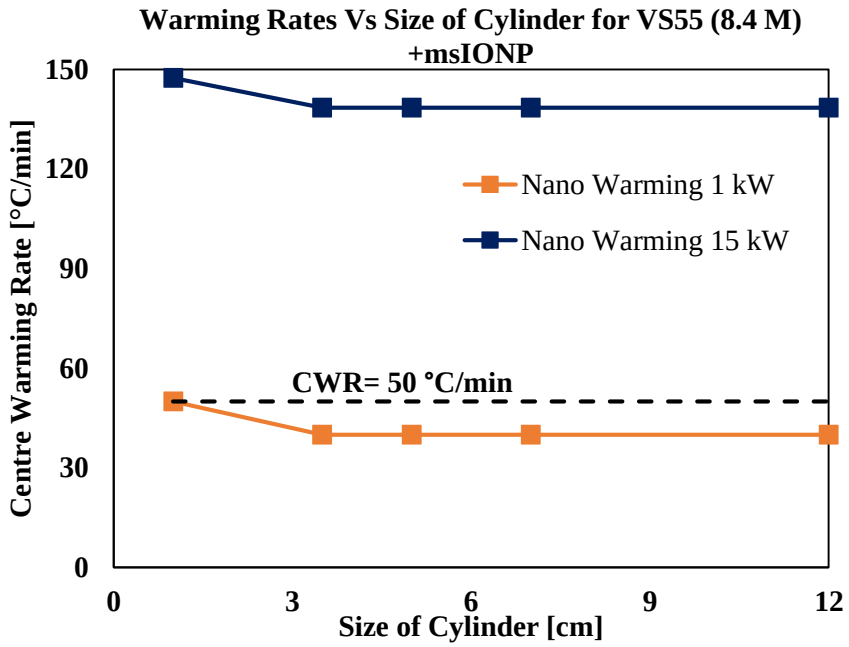

Figure 30. Effect of power input on warming rates for nanowarming in VS55

As seen, the warming rates do not exceed the critical warming rate for VS55 in a 1 kW system beyond volumes of 1 ml or 1 cm in diameter. Hence it was necessary to increase the power of the inductive coil to 15 kW to exceed these warming rates. A power of 15 kW seems sufficient to exceed the critical warming rate for VS55. This power input is sufficient to exceed the critical warming rates for all the CPAs studied except for DP6. DP6 has the highest critical cooling and

Table 10. Centre Warming Rates for Nano-Warming with msIONP

Power [kW]		1	15	15	150	150
CPA	**V [ml]**	1	80	160	500	1300
	D [cm]	1	3.5	5	7	12
	CWR [°C/min]	**Centre Warming Rate [°C/min]**				
VS55	50	50	139	139	398	398
DP6	200	53	150	150	428	428
M22	<1	43	117	117	332	332

warming rates among the studied CPAs owing to its lower concentration (6 M). A similar warming rate plot can be seen in Figure 31 for DP6. As seen, a power input of 1 or 15 kW fails to exceed the critical warming rate for DP6 for all system volumes. Hence a higher power (150 kW) and thus higher volumetric heat generation was tested on DP6 which was able to exceed the critical warming rate. This power is sufficient to exceed the critical warming rates for the CPAs

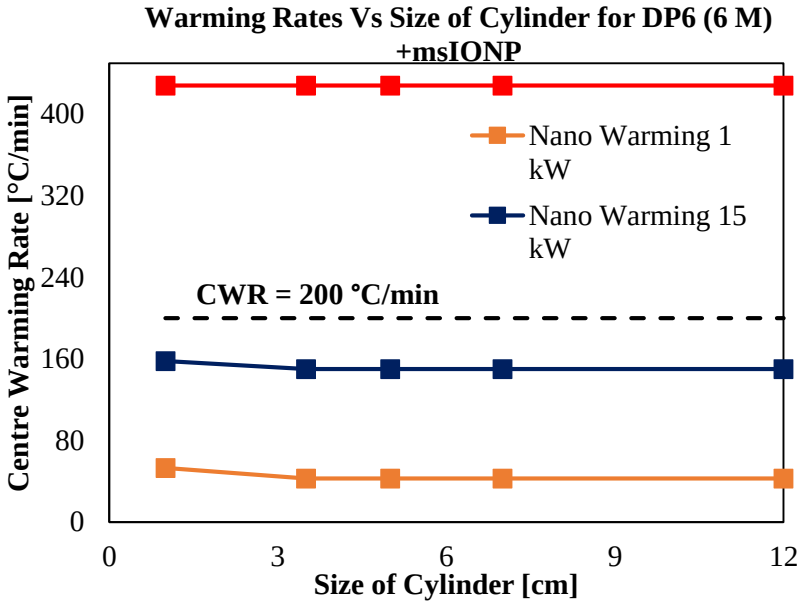

Figure 31. Effect of power input on warming rates for nanowarming in DP6

that have been studied in this project. Hence three power inputs were chosen based on the system volume as indicated in Table 10. This choice of increasing power inputs for increasing volumes is suitable for all CPAs except DP6 which will need a power input of 150 kW for all system volumes. A similar behavior is observed in case of the nanoparticles EMG308 for which data tables are provided in the appendix.

Also as seen in Figures 30 and 31, nano-warming effects for a constant power inputs are size - independent, i.e. the same warming rates are observed across all sizes. The 1 ml volume shows a slightly higher warming rates due to convective boundary conditions imposed on the surface. The convective boundary conditions in addition to nano-warming aided in getting a slightly higher warming rate. For larger sizes, the rates are constant as nano-warming (i.e. heat generation) dominates over convective warming effects. The warming rates will be constant across all volumes if an insulated boundary condition is applied at the outer surfaces. This condition was tested using VS55 properties (Etheridge et al. 2014) to get constant rates for all volumes.

3.4 Conclusion

The modeling study focused on predicting the cooling and warming rates associated with three conditions, viz., convective cooling, convective warming and nano-warming. Convective cooling was successful in terms of the CCR for the CPAs VS55 (up to a volume of 160 ml), M22 (all volumes) and VS55 and DP6 with sucrose (all volumes considering no crystallization at 1°C/min based on DSC studies). DP6 however could not be successfully cooled beyond volumes of 1 ml. Among the three values of convective heat transfer coefficient tested, it was observed that there was no appreciable increase in the cooling rates when the 'h' was increased from 150 to 10,000 W/m^2K. Convective warming resulted in very low warming rates. In terms of CWR it was successful for M22, and VS55 and DP6 with added sucrose due to their lower critical rates. The critical warming rate for sucrose based CPAs is not known. However, they did not crystallize or devitrify for rates of 1,5 and 10 °C/min as was shown in DSC thermograms in Chapter 2. Convective warming was not successful for VS55 and DP6 even in smaller volumes. Due to very slow warming rates as well non-uniform warming in case of convective warming, nano-warming was pursued which provided fast and uniform warming. Among the three power inputs tested, it was observed that a power of 15 kW was sufficient to exceed critical warming rates for all CPAs except DP6 and across all volumes. DP6 due to its lower concentration and thus higher critical warming rates needed a higher power input. A power of 150 kW was seen to produce enough heat generation for all CPAs to exceed their corresponding critical warming rates.

Some future work includes studies to vitrify and nano-warm biological tissues such as arteries perfused with CPAs like VS55 and M22 which are currently being conducted (Manuchehrabadi et al.). Another area which is being pursued (Eisenberg et al. 2016) includes studying the effects of thermal stress which can cause cracking if there are large thermal gradients in the system.

The data tables for cooling and warming rates for the convective cooling / warming and nanowarming for all the CPAs which are not provided in this Chapter have been added to the appendix.

Bibliography

Arkin H, Xu LX, Holmes KR (1994) Recent developments in modeling heat transfer in blood perfused tissues. IEEE Trans Biomed Eng 41:97–107. doi: 10.1109/10.284920

Baish J (2000) Microvascular heat transfer. Biomed Eng Handbook, 98–1.

Balasubramaniam TA, Bowman HF (1977) Thermal Conductivity and Thermal Diffusivity of Biomaterials: A Simultaneous Measurement Technique. J Biomech Eng 99:148. doi: 10.1115/1.3426282

Bald WB, Fraser J (1982) Cryogenic surgery. Reports Prog Phys 45:1381.

Baust JG, Gage AA (2005) The molecular basis of cryosurgery. BJU Int 95:1187–1191. doi: 10.1111/j.1464-410X.2005.05502.x

Belzer FO, Southard JH (1988) Principles of solid-organ preservation by cold storage. Transplantation 45:673–676.

Bhattacharya A, Mahajan RL (2003) Temperature dependence of thermal conductivity of biological tissues. Physiol Meas 24:769–783. doi: 10.1088/0967-3334/24/3/312

Bischof J, Han B (2002) Cryogenic heat and mass transfer in biomedical applications. Heat Transf 1:141–156.

Bowman H (1981) Heat transfer and thermal dosimetry. J Microw Power Electromagn Energy 16:121–133.

Bowman HF, Cravalho EG, Woods M (1975) Theory, Measurement, and Application of Thermal Properties of Biomaterials. Annu Rev Biophys Bioeng 4:43–80. doi: 10.1146/annurev.bb.04.060175.000355

Brockbank KGM, Chen Z, Greene ED, Campbell LH (2015) Vitrification of Heart Valve Tissues. In: Methods in molecular biology (Clifton, N.J.). pp 399–421

Cahill DG, Pohl RO (1987) Thermal conductivity of amorphous solids above the plateau. Phys Rev B 35:4067–4073. doi: 10.1103/PhysRevB.35.4067

Carpenter JF, Pikal MJ, Chang BS, Randolph TW (1997) Rational Design of Stable Lyophilized Protein Formulations: Some Practical Advice. Pharm Res 14:969–975. doi: 10.1023/A:1012180707283

Charny CK (1992) Mathematical Models of Bioheat Transfer. Adv Heat Transf 22:19–155. doi: 10.1016/S0065-2717(08)70344-7

Chato JC (1968) A method for the measurement of the thermal properties of biological materials. In: American Society of Mechincal Engineers: Symposium Series: Thermal Problems in Biotechnology.

Chen MM, Holmes KR, Rupinskas V (1981) Pulse-decay method for measuring the thermal conductivity of living tissues. J Biomech Eng 103:253–260.

Cherneeva LI (1956) Study of thermal properties of foods. In: Report of Vnikhi (Scientific

Research Institute of the Refrigeration Industry), Gostorgisdat, Moscow.

Choi J, Bischof JC (2010) Review of biomaterial thermal property measurements in the cryogenic regime and their use for prediction of equilibrium and non-equilibrium freezing applications in cryobiology. Cryobiology 60:52–70. doi: 10.1016/j.cryobiol.2009.11.004

Choi J, Morrissey M, Bischof JC (2013) Thermal Processing of Biological Tissue at High Temperatures: Impact of Protein Denaturation and Water Loss on the Thermal Properties of Human and Porcine Liver in the Range 25–80 °C. J Heat Transfer 135:61302. doi: 10.1115/1.4023570

Choi JH, Bischof JC (2008a) A quantitative analysis of the thermal properties of porcine liver with glycerol at subzero and cryogenic temperatures. Cryobiology 57:79–83. doi: 10.1016/j.cryobiol.2008.05.004

Choi JH, Bischof JC (2008b) A quantitative analysis on the thermal properties of phosphate buffered saline with glycerol at subzero temperatures. Int J Heat Mass Transf 51:640–649. doi: 10.1016/j.ijheatmasstransfer.2007.04.041

Chu KF, Dupuy DE (2014) Thermal ablation of tumours: biological mechanisms and advances in therapy. Nat Rev Cancer 14:199–208. doi: 10.1038/nrc3672

Crowe JH, Hoekstra FA, Crowe LM (1992) Anhydrobiosis. Annu Rev Physiol 54:579–599. doi: 10.1146/annurev.ph.54.030192.003051

Diller KR (1992) Modeling of Bioheat Transfer Processes at High and Low Temperatures. Adv Heat Transf 22:157–357. doi: 10.1016/S0065-2717(08)70345-9

Diller KR, Valvano JW, Pearce JA (2000) Bioheat transfer. CRC Handb Therm Eng 4:114–215.

Duck FA (2013) Physical properties of tissues: a comprehensive reference book. Academic press

Ehrlich LE, Feig JSG, Schiffres SN, Malen JA, Rabin Y (2015) Large thermal conductivity differences between the crystalline and vitrified states of DMSO with applications to cryopreservation. PLoS One 10:e0125862. doi: 10.1371/journal.pone.0125862

Ehrlich LE, Malen JA, Rabin Y (2016) Thermal conductivity of the cryoprotective cocktail DP6 in cryogenic temperatures, in the presence and absence of synthetic ice modulators. Cryobiology 73:196–202. doi: 10.1016/j.cryobiol.2016.07.012

Eisenberg DP, Bischof JC, Rabin Y (2016) Thermomechanical Stress in Cryopreservation Via Vitrification With Nanoparticle Heating as a Stress-Moderating Effect. J Biomech Eng 138:11010.

Etheridge ML, Choi J, Ramadhyani S, Bischof JC (2013) Methods for Characterizing Convective Cryoprobe Heat Transfer in Ultrasound Gel Phantoms. J Biomech Eng 135:21002. doi: 10.1115/1.4023237

Etheridge ML, Xu Y, Rott L, Choi J, Glasmacher B, Bischof JC (2014) RF heating of magnetic nanoparticles improves the thawing of cryopreserved biomaterials. TECHNOLOGY 2:229–242. doi: 10.1142/S2339547814500204

Fahy GM, MacFarlane DR, Angell CA, Meryman HT (1984) Vitrification as an approach to cryopreservation. Cryobiology 21:407–426. doi: 10.1016/0011-2240(84)90079-8

Fahy GM, Saur J, Williams RJ (1990) Physical problems with the vitrification of large biological systems. Cryobiology 27:492–510. doi: 10.1016/0011-2240(90)90038-6

Fahy GM, Wowk B, Wu J, Phan J, Rasch C, Chang A, Zendejas E (2004) Cryopreservation of organs by vitrification: Perspectives and recent advances. In: Cryobiology. pp 157–178

Gage AA, Baust J (1998) Mechanisms of Tissue Injury in Cryosurgery. Cryobiology 37:171–186. doi: 10.1006/cryo.1998.2115

Glassbrenner CJ, Slack GA (1964) Thermal Conductivity of Silicon and Germanium from 3°K to the Melting Point. Phys Rev 134:A1058–A1069. doi: 10.1103/PhysRev.134.A1058

Grayson J (1952) Internal calorimetry in the determination of thermal conductivity and blood flow. J Physiol 118:54–72.

Guntur SR, Lee K Il, Paeng D-G, Coleman AJ, Choi MJ (2013) Temperature-Dependent Thermal Properties of ex Vivo Liver Undergoing Thermal Ablation. Ultrasound Med Biol 39:1771–1784. doi: 10.1016/j.ultrasmedbio.2013.04.014

Hasgall PA, Di Gennaro F, Baumgartner C, Neufeld E, Gosselin MC, Payne D, Klingenböck A, Kuster N (2015) IT'IS Database for thermal and electromagnetic parameters of biological tissues. Version 3.0, September 1st. 2015.

He X, Bischof JC (2003) Quantification of temperature and injury response in thermal therapy and cryosurgery. Crit Rev Biomed Eng 31:355–422.

He X, Park EYH, Fowler A, Yarmush ML, Toner M (2008) Vitrification by ultra-fast cooling at a low concentration of cryoprotectants in a quartz micro-capillary: A study using murine embryonic stem cells. Cryobiology 56:223–232. doi: 10.1016/j.cryobiol.2008.03.005

Henriques FC, Moritz AR (1947) Studies of Thermal Injury: I. The Conduction of Heat to and through Skin and the Temperatures Attained Therein. A Theoretical and an Experimental Investigation. Am J Pathol 23:530–49.

Hill JE, Leitman JD, JE S (1967) Thermal conductivity of various meats. Food Technol 21:1143-.

Hoffmann NE, Bischof JC (2002) The cryobiology of cryosurgical injury. Urology 60:40–49. doi: 10.1016/S0090-4295(02)01683-7

Höhne GWH, Hemminger W, Flammersheim H-J (1996) Differential Scanning Calorimetry. Springer Berlin Heidelberg, Berlin, Heidelberg

Jin B, Kleinhans FW, Mazur P (2014) Survivals of mouse oocytes approach 100% after vitrification in 3-fold diluted media and ultra-rapid warming by an IR laser pulse. Cryobiology 68:419–430. doi: 10.1016/j.cryobiol.2014.03.005

Karlsson JOM, Toner M (1996) Long-term storage of tissues by cryopreservation: critical issues. Biomaterials 17:243–256. doi: 10.1016/0142-9612(96)85562-1

Kuleshova LL, MacFarlane DR, Trounson AO, Shaw JM (1999) Sugars Exert a Major Influence on the Vitrification Properties of Ethylene Glycol-Based Solutions and Have Low Toxicity to Embryos and Oocytes. Cryobiology 38:119–130. doi: 10.1006/cryo.1999.2153

Lentz CP (1961) Thermal conductivity of meats, fats, gelatin gels, and ice. Food Technol 15:243-.

Liu J, Zhu L, Xu LX (2000) Studies on the Three-Dimensional Temperature Transients in the Canine Prostate During Transurethral Microwave Thermal Therapy. J Biomech Eng 122:372. doi: 10.1115/1.1288208

Lubner SD, Choi J, Wehmeyer G, Waag B, Mishra V, Natesan H, Bischof JC, Dames C (2015) Reusable bi-directional 3ω sensor to measure thermal conductivity of 100-µm thick biological tissues. Rev Sci Instrum 86:14905. doi: 10.1063/1.4905680

Manuchehrabadi N, Gao Z, Zhang J, Ring H., Shao Q, Liu F, McDermott M, Fok A, Rabin Y, Brockbank KG., Garwood M, Haynes C., Bischof J Nanowarming for Regenerative Medicine: Improving Tissue Cryopreservation by Inductive Heating of Magnetic Nanoparticles. ***Accepted for Publication***

Marcus SM, Reading M (1994) Method and apparatus for thermal conductivity measurements.

Mazur P (1984) Freezing of living cells: mechanisms and implications.

Moline SW, RINFRET AP, Short AJ, SAWDYE JA (1961) THERMAL PROPERTIES OF FOODS AT LOW TEMPERATURES. 1. SPECIFIC HEAT. Food Technol 15:228-.

Morley MJ (1966) Thermal conductivities of muscles, fats and bones. Int J Food Sci Technol 1:303–311.

Natesan H, Bischof JC (2016) Multi-Scale Thermal Property Measurements for Biomedical Applications. ACS Biomater Sci Eng acsbiomaterials.6b00565. doi: 10.1021/acsbiomaterials.6b00565

Natesan H, Choi J, Lubner S, Dames C, Bischof J (2016a) Multi-scale Thermal Conductivity Measurements for Cryobiological Applications. In: Multiscale Technologies for Cryomedicine. WORLD SCIENTIFIC, pp 125–171

Natesan H, Hodges W, Choi J, Lubner S, Dames C, Bischof J (2016b) A Micro-Thermal Sensor for Focal Therapy Applications. Sci Rep 6:21395. doi: 10.1038/srep21395

O'Neal DP, Hirsch LR, Halas NJ, Payne JD, West JL (2004) Photo-thermal tumor ablation in mice using near infrared-absorbing nanoparticles.

OPTN Organ Procurement and Transplantation Network - OPTN. https://optn.transplant.hrsa.gov/.

Ozisik N (1994) Finite difference methods in heat transfer. CRC press

Patel PA, Valvano JW, Pearce JA, Prahl SA, Denham CR (1987) A Self-Heated Thermistor Technique to Measure Effective Thermal Properties From the Tissue Surface. J Biomech Eng 109:330. doi: 10.1115/1.3138689

Pennes HH (1948) Analysis of tissue and arterial blood temperatures in the resting human forearm. J Appl Physiol 1:93–122.

Poppendiek HF, Randall R, Breeden JA, Chambers JE, Murphy JR (1967) Thermal conductivity measurements and predictions for biological fluids and tissues. Cryobiology 3:318–327. doi: 10.1016/S0011-2240(67)80005-1

Rabin Y, Shitzer A (1998) Numerical Solution of the Multidimensional Freezing Problem During

Cryosurgery. J Biomech Eng 120:32. doi: 10.1115/1.2834304

Rabin Y, Taylor MJ, Walsh JR, Baicu S, Steif PS (2005) Cryomacroscopy of Vitrification I: A Prototype and Experimental Observations on the Cocktails VS55 and DP6. Cell Preserv Technol 3:169–183. doi: 10.1089/cpt.2005.3.169

Rabin Y, Taylor MJ, Wolmark N (1998) Thermal Expansion Measurements of Frozen Biological Tissues at Cryogenic Temperatures. J Biomech Eng 120:259. doi: 10.1115/1.2798310

Reading M, Hahn BK, Crowe BS (1993) Method and apparatus for modulated differential analysis.

Reading M, Luget A, Wilson R (1994) Modulated differential scanning calorimetry. Thermochim Acta 238:295–307. doi: 10.1016/S0040-6031(94)85215-4

Rossmann C, Haemmerich D (2014) Review of Temperature Dependence of Thermal Properties, Dielectric Properties, and Perfusion of Biological Tissues at Hyperthermic and Ablation Temperatures. Crit Rev Biomed Eng 42:467–492. doi: 10.1615/CritRevBiomedEng.2015012486

Rubinsky B (2000) Cryosurgery. Annu Rev Biomed Eng 2:157–187. doi: 10.1146/annurev.bioeng.2.1.157

Sabel MS (2009) Cryo-immunology: A review of the literature and proposed mechanisms for stimulatory versus suppressive immune responses. Cryobiology 58:1–11. doi: 10.1016/j.cryobiol.2008.10.126

Sapareto SA, Dewey WC (1984) Thermal dose determination in cancer therapy. Int J Radiat Oncol 10:787–800. doi: 10.1016/0360-3016(84)90379-1

Song YC, Khirabadi BS, Lightfoot F, Brockbank KGM, Taylor MJ (2000) Vitreous cryopreservation maintains the function of vascular grafts. Nat Biotechnol 18:296–299. doi: 10.1038/73737

Steponkus PL (1996) Advances in low-temperature biology. Elsevier

Sutton RL (1992) Critical cooling rates for aqueous cryoprotectants in the presence of sugars and polysaccharides. Cryobiology 29:585–598. doi: 10.1016/0011-2240(92)90063-8

Taylor M, Song Y, Brockbank K (2004) 22 Vitrification in Tissue Preservation: New Developments. Life Frozen State, BJ Fuller, NLane, EE Benson, eds, CRC Press Boca Raton, FL 604–641.

Vachon RI, Walker FJ, Walker DF, Nix GH (1967) In vivo determination of thermal conductivity of bone using the thermal comparator technique. In: Digest of the Seventh International Conference of Medical and Biological Engineering. Stockholm, Sweden.

Valvano JW (1995) Tissue Thermal Properties and Perfusion. In: Optical-Thermal Response of Laser-Irradiated Tissue. Springer US, Boston, MA, pp 445–488

Valvano JW, Cochran JR, Diller KR (1985) Thermal conductivity and diffusivity of biomaterials measured with self-heated thermistors. Int J Thermophys 6:301–311. doi: 10.1007/BF00522151

Vendrik AJH, Vos JJ (1957) A Method for the Measurement of the Thermal Conductivity of Human Skin.

Wowk B, Fahy GM (2005) Toward large organ vitrification: extremely low critical cooling and warming rates of M22 vitrification solution. Cryobiology 51:362.

Xu Y, Yu HM, Niu YQ, Luo SC, Cheng X (2016) Effects of Superparamagnetic Nanoparticles on Nucleation and Crystal Growth in the Vitrified VS55 During Warming. Cryo Letters 37:448–454.

Yi F, Kim IK, Li S, Lavan DA (2014) Hydrated/dehydrated lipid phase transitions measured using nanocalorimetry. J Pharm Sci 103:3442–7. doi: 10.1002/jps.24187

Yuan DY, Xu LX, Liang Zhu, Holmes KR, Valvano JW (1998) Perfusion And Temperature Measurements In Hyperthermic Canine Prostates. In: Proceedings of the 17th Southern Biomedical Engineering Conference. 17th Southern Biomed. Eng. Conference, pp 85–85

Zhang H, Cheng S, He L, Zhang A, Zheng Y, Gao D (2002) Determination of Thermal Conductivity of Biomaterials in the Temperature Range 233–313K Using a Tiny Detector Made of a Self-Heated Thermistor. Cell Preserv Technol 1:141–147. doi: 10.1089/153834402320882647

Zhang J, Sandison GA, Murthy JY, Xu LX (2005) Numerical Simulation for Heat Transfer in Prostate Cancer Cryosurgery. J Biomech Eng 127:279. doi: 10.1115/1.1865193

Appendix

Appendix A

Thermal property datasets for thermal conductivity (k) and specific heat capacity (c_p) discussed in Chapter 1 have been provided in this section. Table 3 below, gives a summary of the organization of datasets for porcine and human systems. These dataset tables 4-10 have been classified based on the type of system; i.e. porcine or human, the temperature range considered; i.e. subzero or suprazero, thermal properties of cryoprotectants and effect of cryoprotectants on porcine liver. For porcine liver in Table 6 from (Choi et al. 2013), specific heat data between 31°C-85°C is not directly added as there is an endothermic heat release associated with protein denaturation in that range. The specific heat capacity available in that range is apparent specific heat and not sensible specific heat capacity. The interested reader may refer to (Choi et al. 2013) for more details. The thermal conductivity measurements for porcine and human systems from (Valvano et al. 1985) were carried out at temperatures 3, 10, 17, 23, 37 and 45 °C. Linear regression fit constants were provided to be used in the following formula to calculate thermal conductivity-

$$k = k_0 + k_1 T$$

Where k_0 $\left[\frac{W}{mK}\right]$ and k_1 $\left[\frac{W}{mK^2}\right]$ are regression fit constants and T is the temperature in °C.

Thermal conductivity values have been calculated using the above formula for temperatures 10, 23, 37 and 45 °C.

Appendix Table 1. Organization of thermal property datasets

Appendix Table Number	Description
2 and 3	Porcine Systems at subzero temperatures I and II
4	Porcine Systems at suprazero temperatures
5 and 6	Human Systems at suprazero temperatures I and II
7	Cryoprotectants
8	Porcine liver treated with cryoprotectants

Appendix Table 2. Thermal Properties of Porcine Systems at sub-zero temperatures I

System Type	Thermal Conductivity [W/mK]	Specific Heat Capacity [J/gK]	Reference
Pulmonary Vein	0.57(35.9°C)	3.34(39°C)	'k'— (Natesan et al. 2016b) 'Cp'— Unpublished, BHMT, UMN
	0.47(14.42°C)	3.27(5°C)	
	1.14(-13.77°C)	2.82(1°C)	
	1.44(-30.9°C)	1.87(-34°C)	
	—	1.74(-46°C)	
	—	1.49(-72°C)	
	—	1.38(-84°C)	
Esophagus	0.55(35.58°C)	3.49(39°C)	
	0.48(13.99°C)	3.39(9°C)	
	1.61(-17.43°C)	1.92(-30°C)	
	1.84(-36.95°C)	1.63(-52°C)	
	—	1.43(-74°C)	
	—	1.29(-86°C)	
Phrenic Nerve	0.45(35.53°C)	3.57(33°C)	
	0.5(14.01°C)	3.47(13°C)	
	1.29(-14.01°C)	2.44(-18°C)	
	1.84(-34.18°C)	1.83(-30°C)	
	—	1.7(-44°C)	
	—	1.5(-66°C)	
	—	1.35(-90°C)	

BHMT, UMN: BioheatandMass Transfer Lab, University of Minnesota
n: Number of repetitions

Appendix Table 3. Thermal Properties of Porcine Systems at sub-zero temperatures II

System Type	Thermal Conductivity [W/mK]	Specific Heat Capacity [J/gK]	Reference
Liver	1.6(-11°C)	1.92(-33.3°C)	(Choi and Bischof 2008a)
	1.75(-64°C)	1.6(-65.6°C)	
	1.9(-112°C)	1.171(-113.3°C)	
	2.01(-147°C)	0.95(-144°C)	
Lung	—	3.68(35°C)	Unpublished, BHMT, UMN
	—	3.62(13°C)	
	—	2.04(-26°C)	
	—	1.62(-58°C)	
	—	1.44(-80°C)	
Myocardium (n =3 for 'k', n=8 for 'Cp')	0.5352(37°C)	3.62(50°C)	Unpublished, BHMT, UMN
	0.436(0.1°C)	3.59(30°C)	
	1.743(-26.25°C)	1.75(-34°C)	
	2.046(-94.45°C)	1.508(-62°C)	
	2.312(-147.9°C)	1.241(-98°C)	
Lean, parallel to fiber	1.43(-10°C)	—	(Lentz 1961)
	1.61(-25°C)	—	
	1.23(-10°C)	—	
	1.38(-25°C)	—	
Lean, perpendicular to fiber	0.478(0°C)	—	(Cherneeva 1956)
	0.767(-5°C)	—	
	0.99(-10°C)	—	
	1.29(-20°C)	—	
Lean, neck	0.783(-8°C)	—	(Chato 1968)
	0.835(-8.4°C)	—	
	0.408(-9°C)	—	
Leg	0.49(6°C)	—	(Hill et al. 1967)
	1.28(-8°C)	—	
	1.3(-14°C)	—	
Fat	0.186(0°C)	—	(Cherneeva 1956)
	0.227(-5°C)	—	
	0.254(-10°C)	—	
	0.291(-20°C)	—	
Fat	0.36(-9.1°C)	—	(Chato 1968)
	0.366(-10°C)	—	(Moline et al. 1961)
Exterior (93 % Fat)	0.21(+3 to -24°C)	—	(Lentz 1961)

BHMT, UMN: BioheatandMass Transfer Lab, University of Minnesota
n: Number of repetitions

Appendix Table 4. Thermal Properties of Porcine Systems at supra-zero temperatures

System Type	Thermal Conductivity [W/mK]	Specific Heat Capacity [J/gK]	Reference
Liver	0.5061(10°C)	—	(Valvano et al. 1985)
	0.5165(23°C)	—	
	0.5277(37°C)	—	
	0.5341(45°C)	—	
Lung	0.2561(10°C)	—	
	0.2849(23°C)	—	
	0.3159(37°C)	—	
	0.3336(45°C)	—	
Myocardium	0.4974(10°C)	—	
	0.5148(23°C)	—	
	0.5334(37°C)	—	
	0.5441(45°C)	—	
Pancreas	0.4719(10°C)	—	
	0.4745(23°C)	—	
	0.4772(37°C)	—	
	0.4787(45°C)	—	
Renal Cortex	0.5085(10°C)	—	
	0.5237(23°C)	—	
	0.5402(37°C)	—	
	0.5496(45°C)	—	
Spleen	0.499(10°C)		
	0.5154(23°C)		
	0.5332(37°C)		
	0.5433(45°C)		
Liver	0.4889(25°C)	3.4802(23°C)	(Choi et al. 2013)
	0.5021(37°C)	3.4992(31°C)	
	0.5239(50°C)	3.5864(85°C)	
	0.5479(80°C)	—	
Subcutaneous Fat	0.15-0.17 (30-48°C)	—	(Henriques and Moritz 1947)
Skeletal Muscle	0.43-0.51 (30-48°C)	—	

Appendix Table 5. Thermal Properties of Human Systems at supra-zero temperatures I

System Type	Thermal Conductivity [W/mK]	Specific Heat Capacity [J/gK]	Reference
Renal Pelvis	0.4987(10°C)	—	(Valvano et al. 1985)
	0.5237(23°C)	—	
	0.5507(37°C)	—	
	0.566(45°C)	—	
Renal Medulla	0.5104(10°C)	—	
	0.5247(23°C)	—	
	0.5402(37°C)	—	
	0.549(45°C)	—	
Renal Cortex	0.5118(10°C)	—	
	0.5285(23°C)	—	
	0.5466(37°C)	—	
	0.5569(45°C)	—	
Myocardium	0.5045(10°C)	—	
	0.52(23°C)	—	
	0.5367(37°C)	—	
	0.5463(45°C)	—	
Pancreas	0.4649(10°C)	—	
	0.5019(23°C)	—	
	0.5417(37°C)	—	
	0.5645(45°C)	—	
Lung	0.4189(10°C)	—	
	0.4341(23°C)	—	
	0.4506(37°C)	—	
	0.46(45°C)	—	
Liver	0.4808(10°C)	—	
	0.4959(23°C)	—	
	0.5122(37°C)	—	
	0.5214(45°C)	—	
Spleen	0.5043(10°C)	—	
	0.5212(23°C)	—	
	0.5394(37°C)	—	
	0.5498(45°C)	—	
Cerebral Cortex	0.5083(10°C)	—	
	0.5121(23°C)	—	
	0.5163(37°C)	—	
	0.5186(45°C)	—	
Fat of Spleen	0.3406(10°C)	—	
	0.3373(23°C)	—	
	0.3337(37°C)	—	
	0.3317(45°C)	—	
Liver	0.497(25.6°C)	3.4535(29°C)	(Choi et al. 2013)
	0.51(36.9°C)	3.452(35°C)	
	0.509(49.8°C)	3.4368(39°C)	
	0.519(78.3°C)	—	

BHMT, UMN: Bioheat and Mass Transfer Lab, University of Minnesota

Appendix Table 6. Thermal Properties of Human Systems at supra-zero temperatures II

System Type		Thermal Conductivity [W/mK]	Specific Heat Capacity [J/gK]	Reference
Kidney (n≥5)		0.591(25°C)	—	Unpublished, BHMT, UMN
		0.585(37°C)	—	
		0.56(50°C)	—	
		0.555(80°C)		
Liver		0.467-0.527(37°C)	—	(Bowman 1981)
Lung		0.302-0.55(37°C)	—	
Pancreas		0.294-0.588(37°C)	—	
Kidney		0.513-0.564(37°C)	—	
Heart		0.492-0.562(37°C)	—	
Spleen		0.448-0.544(37°C)	—	
Stomach		0.489-0.565(37°C)	—	
Skeletal Muscle		0.449-0.546(37°C)	—	
Adrenal Gland		0.363-0.458(37°C)	—	
Colon		0.556(37°C)	—	
Brain (white-gray)		0.503-0.576(37°C)	—	
Thyroid		0.526-0.533(37°C)	—	
Breast		0.499(37°C)	—	
Bone (rib)		0.373-0.496(37°C)	—	
Skin (Without SF)		0.258-0.272(37°C)	—	
Fat		0.2-0.246(37°C)	—	
Skin	1.6 mm	0.498(37°C)	—	
Fat	4.8 mm	0.268(37°C) (surface of fat)	—	
Fat	6.4 mm	0.248(37°C) (intermediate fat)	—	
Fat	9.8 mm	0.219(37°C) (deeper fat)	—	
Mesentery (n≥13)		0.303(25°C)	—	Unpublished, BHMT, UMN
		0.279(37°C)	—	
		0.242(50°C)	—	
		0.243(80°C)	—	
Omentum (n≥8)		0.26(25°C)	—	
		0.299(37°C)	—	
		0.251(50°C)	—	
		0.237(80°C)	—	
Gerota's Fascia (n≥2)		0.324(25°C)	—	
		0.279(37°C)	—	
		0.255(50°C)	—	
		0.178(80°C)	—	

BHMT, UMN: BioheatandMass Transfer Lab, University of Minnesota
SF: Subcutaneous Fat
n: Number of repetitions

Appendix Table 7. Thermal Properties of Cryoprotectants

System Type	Thermal Conductivity [W/mK]	Specific Heat Capacity [J/gK]	Reference
US Gel (Tissue Phantom)	0.52(38°C)	3.7(39°C)	(Etheridge et al. 2013)
	0.47(-2°C)	3.84(10°C)	
	1.71(-45°C)	2.06(-50°C)	
	2.3(-85°C)	1.45(-100°C)	
	2.28(-125°C)	0.94(-149°C)	
2M Glycerol Solution	1.61(-27°C)	3.781(-5°C)	(Choi and Bischof 2010)
	1.96(-64°C)	1.712(-73°C)	
	2.15(-108°C)	1.206(-110°C)	
	2.25(-147°C)	0.903(-148°C)	
6M Glycerol Solution	0.82(-28°C)	2.984(-20°C)	
	1.27(-65°C)	1.996(-73°C)	
	1.05(-108°C)	1.114(-110°C)	
	0.97(-147°C)	0.834(-148°C)	
2M DMSO Solution	1.443(-20°C)	—	(Ehrlich et al. 2015)
	1.69(-60°C)	—	
	1.933(-100°C)	—	
	2.203(-140°C)	—	
6M DMSO Solution	0.378(-20°C)	—	
	0.592(-60°C)	—	
	0.721(-100°C)	—	
	0.773(-140°C)	—	
10M DMSO Solution	0.28(-20°C)	—	
	0.27(-60°C)	—	
	0.264(-100°C)	—	
	0.253(-140°C)	—	
DP6 in EC Solution (cryoprotectant)	0.317(-20°C)	—	(Ehrlich et al. 2016)
	0.53(-40°C)	—	
	0.356(-70°C)	—	
	0.35(-140°C)	—	

Appendix Table 8. Thermal Properties of Porcine Liver treated with cryoprotectants

System Type	Thermal Conductivity [W/mK]	Specific Heat Capacity [J/gK]	Reference
Porcine Liver, treated with 1X PBS + 2M Glycerol	1.56(-10°C)	3.39(20°C)	(Choi and Bischof 2008a)
	1.68(-64°C)	3.36(3.7°C)	
	1.78(-108°C)	3.09(-7.3°C)	
	1.73(-146°C)	2.55(-13°C)	
	—	2.1(-36°C)	
	—	1.85(-57.2°C)	
	—	1.58(-72.8°C)	
	—	1.45(-89°C)	
	—	1.17(-104.9°C)	
	—	0.8638(-143.8°C)	
Porcine Liver, treated with 1X PBS + 6M Glycerol	1.0(-13°C)	3.03(23.5°C)	
	1.55(-64°C)	2.91(-8.5°C)	
	1.42(-110°C)	2.81(-24.3°C)	
	1.24(-148°C)	2.51(-43.6°C)	
	—	2.28(-57.4°C)	
	—	1.94(-82.2°C)	
	—	1.76(-98.3°C)	
	—	1.33(-106°C)	
	—	1.05(-114.4°C)	
	—	0.83(-145.8°C)	
Porcine Liver, treated with 1X PBS + 8M Glycerol	0.65(-10°C)	2.91(20.3°C)	
	1.27(-64°C)	2.69(-23.2°C)	
	1.07(-109°C)	2.42(-36.2°C)	
	0.86(-149°C)	2.15(-56.2°C)	
	—	1.9(-83.4°C)	
	—	1.62(-103°C)	
	—	2.51(-43.6°C)	
	—	1.19(-111.2°C)	
	—	0.96(-118.7°C)	
	—	0.81(-142.8°C)	

Appendix B

B.1 DSC Protocol for Maximal Crystallization Measurements

(This protocol has been adapted from (Choi and Bischof 2008b))

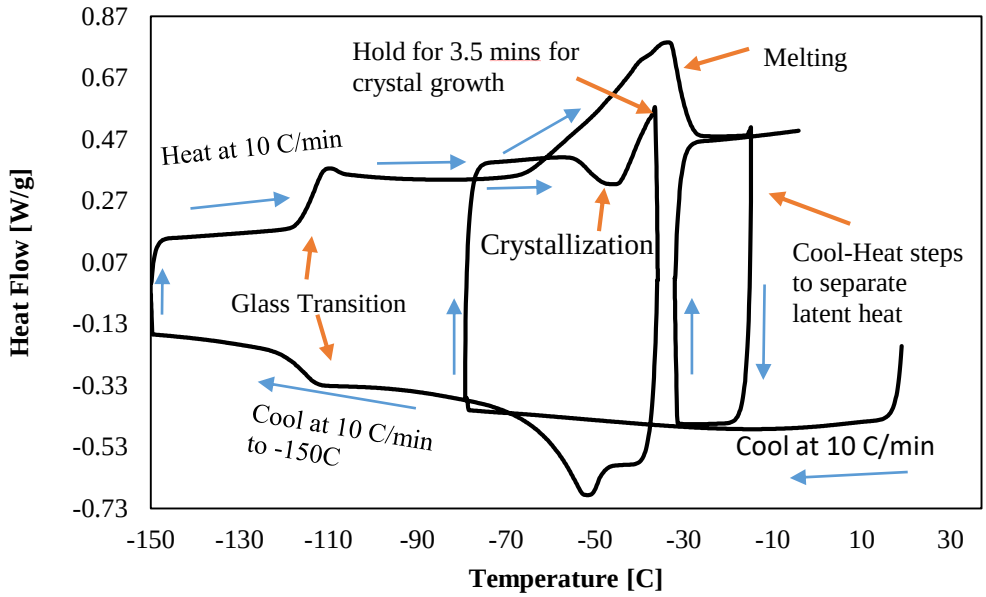

Appendix Figure 1. Thermogram for maximal crystallization

The thermogram provided in Appendix Figure 1 can be explained as follows:

A cooling and warming rate of 10°C/min was used for DP6 whereas a rate of 5°C/min as used for VS55 as explained below.

For maximally crystallized measurements, the sample needs to be nucleated and the crystals are allowed to grow as explained in Chapter 2. The thermogram above has been provided for DP6. DP6 does not crystallize when cooled at 10°C/min when used in the TA Q1000 DSC. Hence it was first cooled to an intermediate temperature (~ -80°C) and then heated back up. This first leads to a crystallization event as seen in the figure. The sample needs to be heated up to a temperature closest to the peak temperature seen when the sample is being melted. This should first be tested to get the melt temperature by doing a simple cool-heat cycle. The sample needs to be then held at this near peak temperature for a duration of 3-3.5 mins for the crystal growth step. It then is cooled down to -150°C/min and held there for 2-3 mins. VS55 also does not crystallize at 10 °C/min (being > CCR) and hence needs to be cooled and heated up similar to DP6. It was observed that cooling down to -90°C and heating back up did not initiate crystallization while heating as seen for DP6. The sample had to be cooled to -150°C and then heated to get the crystallization peak. The steps further are the same as explained for DP6. Also, for VS55, a small

devitrification peak was observed at a rate of 10°C/min when heated up after the crystallization, crystal growth and cool down to -150°C steps had been completed. This showed that maximal crystallization had not occurred prior to the heating step for c_p measurement. Hence a rate of 5°C/min was used to avoid this devitrification peak and ensure maximal crystallization before the final heating step to measure c_p.

While heating, the c_p data can be collected just before the beginning of melting (around -70°C) in the thermogram above. c_p data in the melt region needs to be calculated as shown in Chapter 2 due to the evolution of latent heat. Post melting, the sample can be cooled back to the point where melting has finished (around -30°C) and can be heated back up to 0°C to measure c_p data in the range of -30°C to 0°C. This cool-heat step instead of direct data collection post melt is applied in order to remove latent heat effects from the data. The DSC was not stable at temperatures above 0°C and hence data was not collected in the 0-37°C range. Also a water correction was multiplied to the c_p data to correct for slope differences. Hence 2-3 measurements for the c_p of water need to be performed on each day of actual measurements to account for the slope differences on that particular day. The protocol for water measurements should be the same as was used for CPA measurements. The exact DSC protocol followed has been provided below.

OrgMethod 1: Data storage On
OrgMethod 2: Sampling interval 1.00 s/pt
OrgMethod 3: Equilibrate at 20.00 °C
OrgMethod 4: Ramp 10.00 °C/min to -80.00 °C
OrgMethod 5: Ramp 10.00 °C/min to -35.80 °C
OrgMethod 6: Isothermal for 3.50 min
OrgMethod 7: Ramp 10.00 °C/min to -150.00 °C
OrgMethod 8: Isothermal for 2.00 min
OrgMethod 9: Mark end of cycle 1
OrgMethod 10: Ramp 10.00 °C/min to -73.00 °C
OrgMethod 11: Mark end of cycle 2
OrgMethod 12: Ramp 10.00 °C/min to -14.00 °C
OrgMethod 13: Ramp 10.00 °C/min to -32.00 °C
OrgMethod 14: Isothermal for 2.00 min
OrgMethod 15: Mark end of cycle 3
OrgMethod 16: Ramp 10.00 °C/min to -2.50 °C
OrgMethod 17: Mark end of cycle 4

The Data Storage ON step is needed to allow the system to collect the heat flow data. The Mark end of Cycle step simply allows for creating separate steps from which data can be collected. This makes it easier to separate all the cooling and warming steps used for crystallization and growth from the final heating steps which contain the C_p data that was measured.

B.2 DSC c_p Datasets of CPAs not shown in Chapter 2.

B.2.1 c_p data for DP6 in the maximal and minimal modes of crystallization.

The c_p behavior shown in Appendix Figure 2, is similar to that explained for VS55 in Chapter 2.

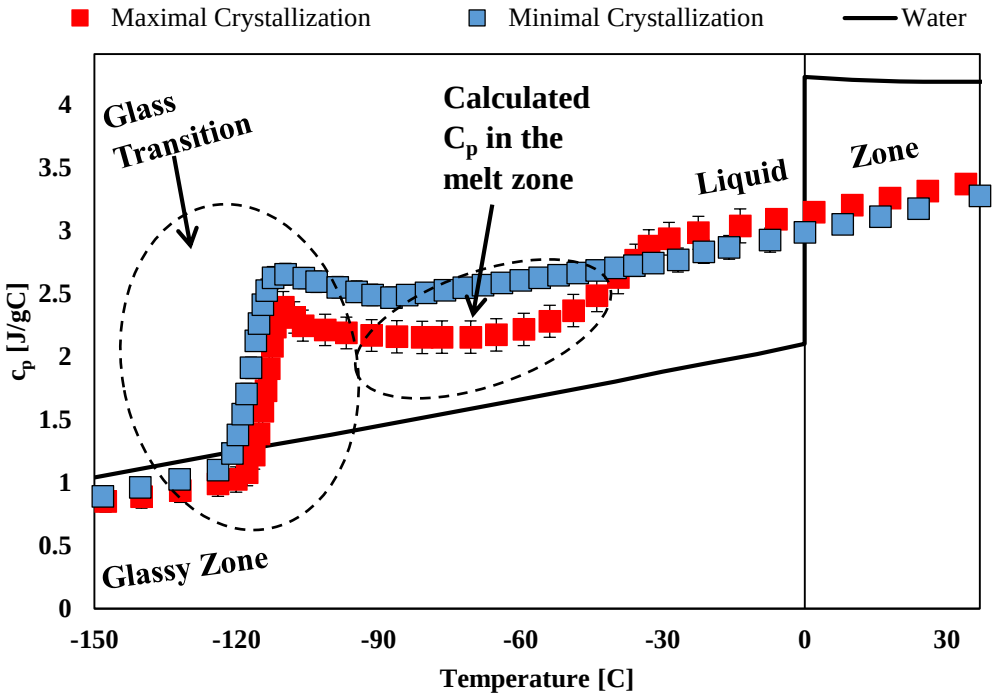

Appendix Figure 2. c_p for DP6 for maximal and minimal modes of crystallization

B.2.2 c_p data for DP6 with and without 0.6M Sucrose.

The c_p behavior seen in Appendix Figure 3, is similar to that explained for VS55 with 0.6 M Sucrose in Chapter 2. Except for an increase in glass transition temperature, there is negligible difference in the c_p values for DP6 with and without 0.6 M sucrose. The c_p values for VS55 + 0.6M sucrose were consistently below those for VS55 as seen in Chapter 2.

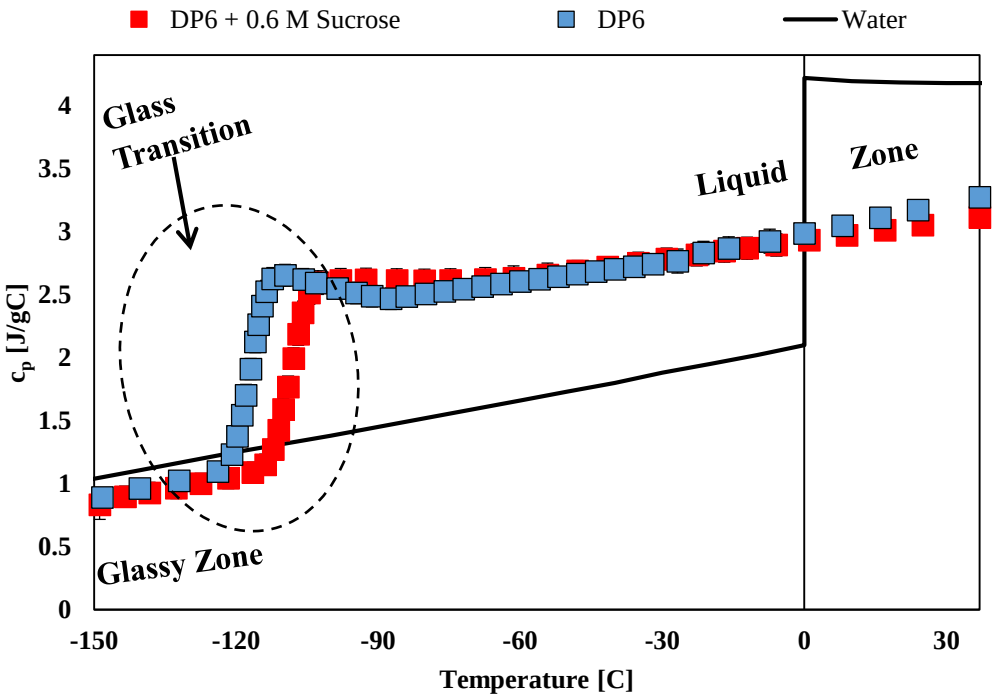

Appendix Figure 3. Specific Heat Capacity (c_p) of DP6 and DP6 + 0.6 M Sucrose

B.2.3 Summary of c_p measurements for maximal and minimal crystallization conditions

Following are the maximal and minimal crystallization measurements for VS55, DP6 and M22. M22 was only measured for minimal crystallization as it does not crystallize at practical DSC scanning rates due to very low critical cooling and warming rates.

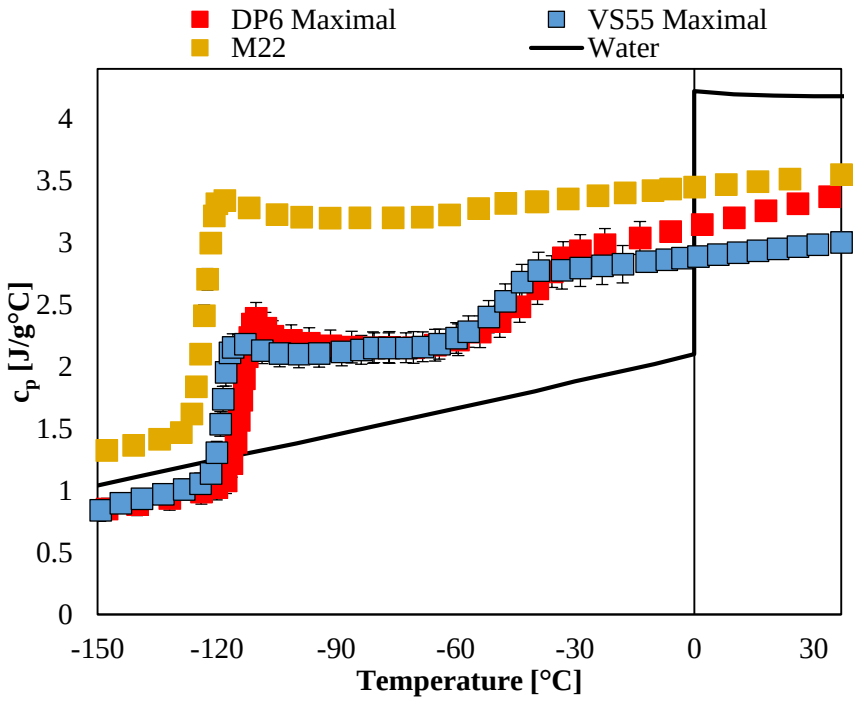

Appendix Figure 4. Specific Heat Capacity (c_p) for maximal crystallization measurements

Comparing between appendix Figures 4 and 5, the minimal crystallization measurements see a higher rise in the specific heat capacity during glass transition for VS55 and DP6. The reason for this is there is going to be more liquid content in the minimally crystallized scenario as compared to the maximal crystallized scenario. Also as seen, the liquid water has a higher specific heat capacity than ice. Thus as glass transitions into liquid, the maximally crystallized condition will have a smaller liquid region as most of the system is crystallized while the amount of glass transition into liquid is going to be higher for the minimally crystallized condition. Hence this increase in the specific heat capacity during glass transition is smaller as seen in Appendix Figure 4 for the maximally crystallized condition.

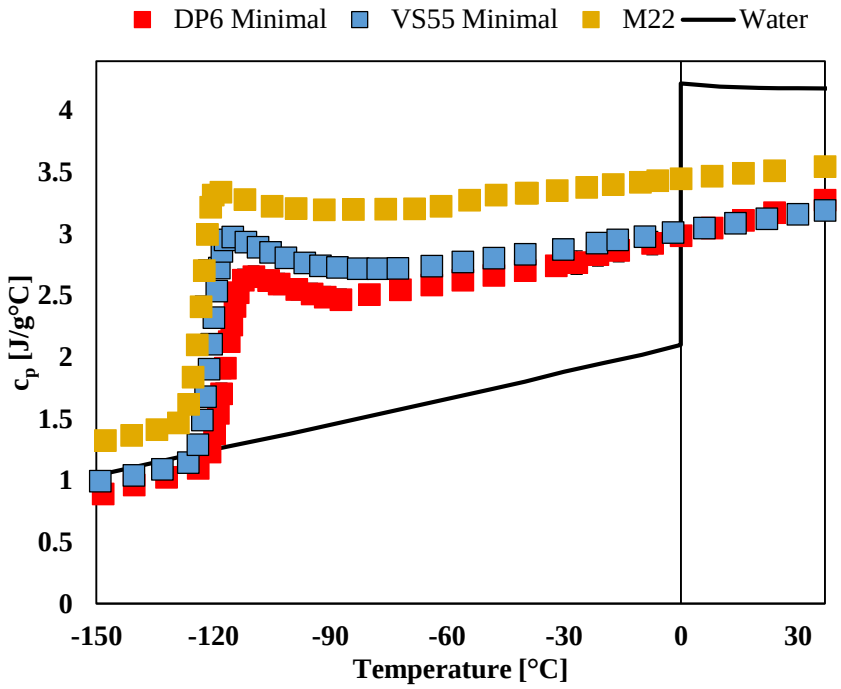

Appendix Figure 5. Specific Heat Capacity (c_p) for minimal crystallization measurements

Appendix C

C.1 Convective Cooling Results for VS55 and DP6 with 0.6 M Sucrose

As seen in Appendix Table 9, the cooling rates were consistently greater than 1°C/min except for 1.3L systems for VS55 and DP6 with 0.6 M sucrose. No crystallization or melting was observed

Appendix Table 9. Centre Cooling Rates for Convective Cooling

CPA	V [ml]	1	80	160	500	1300
	D [cm]	1	3.5	5	7	12
	h [W/m^{2}K]	Centre Cooling Rate [°C/min]				
VS55+0.6M Sucrose [CCR:NA]	15	18.2	2.7	1.82	1.07	0.58
	150	78	7.2	3.9	2.01	0.88
	10000	133	8.9	4.5	2.24	0.94
DP6+0.6M Sucrose [CCR:NA]	15	17.1	2.7	1.8	1.05	0.57
	150	76	7.1	3.9	2	0.9
	10000	133	8.7	4.5	2.22	0.94
M22 [CCR: <1 °C/min]	15	13	2.1	1.4	0.81	0.4
	150	58.3	5.5	3	1.54	0.7
	10000	100	6.7	3.4	1.71	0.71

during DSC measurements at a rate of 1°C/min for these CPAs. This is shown in Table 13 in Chapter 2. The rates consistently exceeded CWR in case of M22.

C.2 Convective Warming Results for VS55 and DP6 with 0.6 M Sucrose.

As seen in Appendix Table 10, the warming rates exceeded 1°C/min for all systems except the case of 1.3 L. No crystallization or melting was observed during DSC measurements at a rate of 1°C/min for these CPAs. This is shown in Table 13 in Chapter 2.

Appendix Table 10. Centre Cooling Rates for Convective Warming

CPA	V [ml]	1	80	160	500	1300
	D [cm]	1	3.5	5	7	12
	CWR [°C/min]	Centre Warming Rate [°C/min]				
VS55*	<1	26.2	3.9	2.5	1.42	0.7
DP6*	<1	25.4	3.8	2.4	1.37	0.7

*— With 0.6 M Sucrose

C.3 Nano-Warming Results for VS55 and DP6 with 0.6 M Sucrose using msIONP

The warming rates as seen in Appendix Table 11, exceed 1°C/min for all cases. No crystallization or melting was observed during DSC measurements at a rate of 1°C/min for these CPAs. This is shown in Table 13 in Chapter 2.

Appendix Table 11. Centre Warming Rates for Nano – Warming with msIONP

Power [kW]		1	15	15	150	150
CPA	V [ml]	1	80	160	500	1300
	D [cm]	1	3.5	5	7	12
	CWR [°C/min]	Centre Warming Rate [°C/min]				
VS55*	<1	56	160.7	158	453	453
DP6*	<1	56	155.2	158	443	443

*— With 0.6 M Sucrose

C.4 Nano-Warming Results for all CPAs using EMG308 Nano-particles.

As seen in Appendix Table 12 below, only DP6 failed to exceed CWR up to a volume of 160 ml. A power of 150 kW was sufficient to exceed the CWR's of all CPAs.

Appendix Table 12. Centre Warming Rates for Nano – Warming with EMG308

Power [kW]		1	15	15	150	150
CPA	**V [ml]**	1	80	160	500	1300
	D [cm]	1	3.5	5	7	12
	CWR [°C/min]	**Centre Warming Rate [°C/min]**				
VS55	50	65	152.5	152.5	553.8	552.1
DP6	200	69	163.6	165.1	592.1	592.1
M22	<1	55	130.4	127.7	466.3	466.3
VS55*	<1	73	173	173	629.4	629.4
DP6*	<1	71	173	171	616.4	616.4

*— With 0.6 M Sucrose